21 SEVERE ACCIDENT MANAGEMENT

Contents

Abbreviations and Acronyms

ADS	Automatic Depressurization System
ALWR	Advanced Light Water Reactor
ATWS	Anticipated Transients Without Scram
BiMAC	Basemat Internal Melt Arrest and Coolability (Device)
BMP	Basemat Melt Penetration
BWR	Boiling Water Reactor
CBP	Containment Bypass and Leakage
CCFP	Conditional Containment Failure Probability
CCI	Corium-Concrete Interactions
CDF	Core Damage Frequency
CET	Containment Event Tree
CLCH	Convection-Limited Containment Heating (model for DCH)
COP	Containment Over-Pressurization
CPET	Containment Phenomenological Event Tree
CRD	Control Rod Drive
CRSS	Center for Risk Studies and Safety
CSET	Containment Systems Event Tree
CV	Containment Vessel
DCD	Design Control Document
DCH	Direct Containment Heating
DPV	Depressurization Valve
DW	Drywell
EPRI	Electric Power Research Institute
EVE	Ex-Vessel Steam Explosion
FCI	Fuel-Coolant Interaction
GDCS	Gravity-Driven Cooling System
GEH	GE Hitachi
GE-NE	GE Nuclear Energy
H2C	Hydrogen Combustion
HP	High Pressure (core-melt Scenario)
HPME	High Pressure Melt Ejection
I&C	Instrumentation and Control
ICS	Isolation Condenser System
IGT	Instrumentation Guide Tube
IVR	In-Vessel Retention (severe accident management scheme)
LDW	Lower Drywell

LOCA	Loss of Coolant Accident
LP	Low Pressure (core-melt scenario)
MAAP	Modular Accident Analysis Program
MCCI	Molten Corium-Concrete Interactions
MCOPS	Manually Operated Containment Overpressurization System
MSIV	Main Steam Isolation Valve
MSL	Main Steam-Line
NRC	Nuclear Regulatory Commission
O&M	Operation and Maintenance
PCC	Passive Containment Cooling
PCCS	Passive Containment Cooling System
PRA	Probabilistic Risk Assessment
PSA	Probabilistic Safety Assessment
PWR	Pressurized Water Reactor
ROAAM	Risk-Oriented Accident Analysis Methodology
RCCV	Reinforced Concrete Containment Vessel
RPV	Reactor Pressure Vessel
SA	Severe Accident
SAM	Severe Accident Management
SBWR	Simplified Boiling Water Reactor
SP	Suppresssion Pool
SRV	Safety Relief Valve
TDH	Torispherical Drywell Head
UCSB	University of California, Santa Barbara (CRSS)
UDW	Upper Drywell
URD	Utility Requirement Documents
VB	Vacuum Breaker

List of Tables

List of Figures

21.0 SEVERE ACCIDENT MANAGEMENT

Executive Summary

A central concern of Severe Accident Management (SAM) in ESBWR was in-containment stabilization of melt progression, and coolability of the resulting core debris in a manner convenient to post accident recovery. This concern was addressed by inventing, designing, and incorporating the Basemat- Internal Melt Arrest and Coolability (BiMAC) device. In Section 21.5 we present activation and functional requirements of this device, and show that it would robustly intervene in all risk-significant Severe Accident (SA) sequences to present a melt-containing, impenetrable boundary, thus assuring long-term coolability, and absence of melt-concrete interactions and Basemat Melt Penetration (BMP).

The BiMAC device consists of a liner-like arrangement of a series of steel pipes that cover the LDW floor and side walls to a height of ~2 m (~7 ft). Flow inside these pipes is gravity-driven from the GDCS pools and it is established initially by activation of several LDW deluge lines, and by natural circulation once the water level in the LDW has risen to a height of ~2 m (~7 ft) ~3 min. The activation requirement is that deluge line valves meet a 0.999 reliability criterion both in opening up on demand (immediately following vessel breach), and against opening up prematurely (prior to vessel breech). In addition, there will be a diverse/passive deluge system. [The diverse/passive deluge system has been deleted with the implementation of squib-actuated valves in the deluge system as described in ESBWR DCD Tier 2, Section 6.3.2.7.] Functional requirements of BiMAC are that local Burnout (due to the thermal load exceeding the Critical Heat Flux, or CHF) as well as global flow conditions that lead to local dry-outs (due to flow instability) are avoided with great margins. While optimization of the design parameters is yet to be performed (along with experiments), we are able to show that the concept is in principle sound, and such margins will be possible to verify at a high level of confidence. Furthermore, the design includes a (minimum of) 20 cm (7.9 in) thick, (sacrificial) refractory layer which we show to effectively protect the BiMAC pipes under all conceivable conditions of melt release from the reactor pressure vessel. In this document we also treat (by analysis) Direct Containment Heating (DCH), due to melt dispersal from RPV failure at high pressure (the Class III, or HP scenarios), and Ex-Vessel Steam Explosions (EVE). For the former we examine energetic DW over-pressurization as well as the thermally stressed UDW liner, and we find that containment failure in both cases is physically unreasonable. For the latter we find, in a conservative treatment, that (a) fuel-coolant interactions in shallow, saturated water pools would be of no structural concern, and (b) the potential pulses from explosions in deep (> 1.5 m, 4.9 ft), subcooled water pools, receiving melt pours in the typical range of 100's of kg/s, could exceed the structural capacity of both the reactor pedestal wall, as well as that of the BiMAC. These outcomes we assume to constitute containment failure.

[1]Information in [ ] reflect updated information from Revision 4 of the ESBWR PRA. The ESBWR PRA, Level 1 and 2, will continue to be revised. Changes to the methodology in this section, Severe Accident Management, are not expected.

This work was performed under the overall philosophy of the Risk Oriented Accident Analysis Methodology (ROAAM), and it has benefited from prior work on SAM carried out for the US NRC (on SA issue resolution for existing plants), and US DOE (on the AP-600, and AP-1000).

This section consists of two introductory sections on ESBWR design and methodology of SAM, and three main sections addressing DCH, EVE, and BMP (BiMAC) respectively. There is also an addendum with the reviewer reports and our responses.

21.1 OVERVIEW OF ESBWR DESIGN FEATURES TO ELIMINATE HYPOTHETICAL SEVERE ACCIDENT THREATS TO CONTAINMENT INTEGRITY

The results of Level 1 PRA (GE-NE, 2005a) show that core damage events (Severe Accidents) in ESBWR are remote and speculative (CDF~10^{-8}). Still, efforts have been made, and design features and procedures have been included that provide an additional (diverse and redundant) layer of defense against all threats to containment integrity that such hypothetical events may conceivably entail.

Given a severe accident, threats to containment integrity may be enumerated as follows:

a. Prompt, Energetic Loading: Explosive fuel-coolant interactions, high pressure melt ejection leading to direct containment heating (and pressurization);

b. Late, Gradual Loading: Melt ablation and penetration of the containment basemat, pressurization of containment atmosphere by steam and/or non-condensable gases, and;

c. Isolation Failure: Errors or malfunctions that leave existing flow paths open to the outside, activation of the containment overpressure protection system.

In this report we will deal with the phenomenological (physics) components of these threats; namely, Ex-vessel Steam Explosions (EVE), Direct Containment Heating (DCH), and Basemat Melt Penetration (BMP). Our treatment of the BMP will also provide the principal phenomenological input needed to assess Containment Over-pressurization, which, being a systems-driven event, is treated in the Level 2 PRA. This is the case for Isolation Failure as well.

From a top level perspective a principal strategic decision we had to make for Severe Accident Management (SAM) in the ESBWR was in regards to arresting the melt propagation process and ensuring long term coolability within the containment boundary. As one potential option we examined the applicability and effectiveness of In-Vessel Retention (IVR)—an internationally pursued severe accident management approach, already developed and utilized for the passive PWR designs in the USA (Theofanous et al, 1996). We concluded that this could be a highly effective approach for the ESBWR as well, however, only if all equipment found hanging from the lower head penetrations were to be supported from the outside so as to maintain the melt-containing capacity of the lower head. This proved unworkable from the operational perspective, and the option was rejected by the design managers. On the other hand, we determined that the coolability question could be addressed ex-vessel and with a high degree of certainty. Thus ex-vessel behavior is the principal focus of our treatment in this report. More specifically, we are to address manifestations of the above noted threats to containment integrity in a manner that is inclusive of all possible ex-vessel evolutions. Our approach is comprehensive and founded on the basic physics that underlie these evolutions.

As in the most recent ABWR design, the ESBWR features: an inert containment atmosphere to prevent deflagration or detonation of combustible mixtures; a Containment Over-pressurization Protection System (COPS) (but here it is manually operated—MCOPS) to guard against slow buildup of pressure due to non-condensable gas generation and/or heat-up of the suppression pool water; and a drywell spray system in support of accident recovery operations. Unlike the ABWR, or any other previous GE BWR, the ESBWR containment design includes the Passive Containment Cooling System (PCCS), to remove decay heat from the containment, and the (also

passive) Basemat-Internal Melt Arrest and Coolability (BiMAC) device (invented in the course of this work— Theofanous and Dinh, 2005), to essentially eliminate the possibility of extended corium-melt interactions, non-condensable gas generation, and base-mat penetration. In addition, the ESBWR is equipped with the Isolation Condensors (IC's), a system for ensuring decay heat removal from the RPV in sequences where the reactor is at high pressure. This is an improved version of system employed in some of the earlier BWR designs.

An overall illustration that summarizes all these systems in the framework of the ESBWR containment can be found in Figure 21.1-1. Detailed descriptions and performance assessments under severe accident conditions are provided in Sections 21.3 through 21.5. Containment Phenomena Event Trees (CPETs) provide for all necessary links to the relevant/consistent sets of Plant Damage States (PDSs) through the Level 1 PRA (GE-NE, 2005a), and to Containment Systems Event Trees (CSETs) and potential release categories as employed in Levels 2 and 3 PRA (GE-NE, 2005a). The overall assessment methodology is summarized in the next Section.

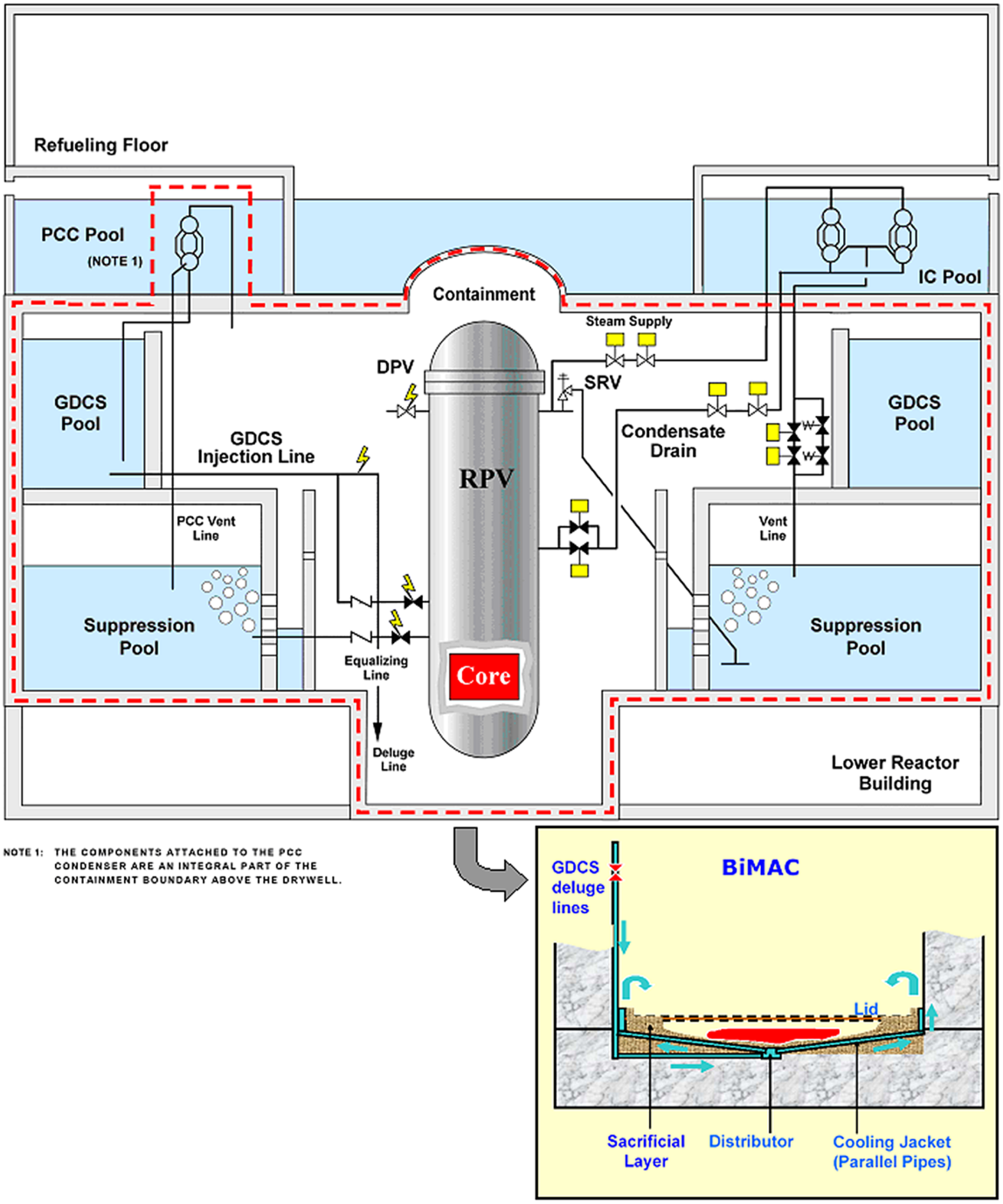

Figure 21.1-1. ESBWR Design Features for Severe Accident Conditions

The design features are aimed for ensuring containment integrity under severe accident conditions. From top down: (i) PCCS pool and heat exchangers, operated on DW-to-WW pressure difference provide passive containment cooling, (ii) IC pool and heat exchangers provide decay heat removal from RPV; (iii) GDCS (three pools, four divisions) with ADS (DPV, SRV) make up the ECCS; LDW deluge lines feeding off the GDCS supply the BiMAC for long-term coolability; (iv) Manual COPS (MCOPS), not shown, provides venting from wetwell,

through 2” (50 mm) and 12” (300 mm) vents, in a controlled manner; (v) Basemat-Internal Melt Arrest and Coolability (BiMAC) device (shown in the bottom insert). It is initially fed by water flow from squib-valve-operated (along with some other type of valve for diversity—not shown in the figure) LDW deluge lines [The diverse/deluge system has been deleted with the implementation of squib-actuated valves in the deluge system as described in ESBWR DCD Tier 2.], while in the long term it is supplied by natural circulation, through downcomers (at the edges of LDW, not shown in the insert).

21.1.1 Assumptions and Insights

The following assumptions were made concerning the threats to containment integrity during the development of the ESBWR Severe Accident Management. They are discussed and analyzed further in the following sections. Since they form the basis of this analysis, they are key. However, they have been analyzed in this document and reviewed using Risk Oriented Accident Analysis Methodology as described in Section 21.2 and found acceptable.

(1) Ex-vessel Steam Explosions are only relevant to low pressure scenarios.

(2) Direct Containment Heating is only relevant to high pressure scenarios.

(3) Basemat Melt Penetration is relevant to both low and high pressure scenarios.

(4) Combustion in containment is not a concern since the containment is inerted. [Combustible gas accumulation in PCCS and ICS is addressed in the Level 2 PRA – see Section 8.]

(5) Natural depressurization due to creep rupture of Main Steam lines is not credited.

The following insight is obtained from the ESBWR Severe Accident Management:

(6) The ESBWR containment is designed to minimize the effects of direct containment heating, ex-vessel steam explosions, and core-concrete interaction.

21.1.2 References

21.1.-1 GE-NE (2005a), ESBWR Certification Probabilistic Safety Assessment, NEDC-33201P, August 2005.

21.1.-2 GE-NE (2005b), ESBWR Design Control Document, 26A6642BZ Rev.00. August 2005.

21.1.-3 Theofanous, T.G., Liu, C., Additon, S., Angelini, S., Kymalainen O., and Salmassi, T. (1996), “In-Vessel Coolability and Retention of a Core Melt,” DOE/ID-10460, Vols. 1 and 2, October 1996. Also in:

21.1.-4 Theofanous, T.G., Liu, C., Additon, S., Angelini, S., Kymalainen O., and Salmassi, T. “In-Vessel Coolability and Retention of a Core Melt,” Nuclear Engineering & Design, 169 (1997) 1–48.

21.1.-5 Theofanous T.G., and Syri, S., “The Coolability Limits of a Reactor Pressure Vessel Lower Head,” Nuclear Engineering & Design 169 (1997) 59–76.

21.1.-6 Theofanous, T.G. and Dinh, T.N., “Basemat-Internal Melt Arrest and Coolability (BiMAC) device”. Patent Application. TcI/GE Document. GE Nuclear Energy. San Jose, March 30, 2005.

21.2 ROAAM-BASED TREATMENT OF CONTAINMENT THREATS; INTERFACES TO LEVELS 1&2 PRA

The Risk Oriented Accident Analysis Methodology (ROAAM) was developed for the purpose of resolving "issues" that proved hard to address in a purely probabilistic (PRA) framework (Theofanous, 1996). This purpose was met mainly due to a methodological emphasis on deterministic principles (key physics) along with an overall conservative mentality of treatment. Accordingly, principal ingredients of ROAAM include: (a) identification, separate treatment, and maintenance of this separation (to the end results), of Aleatory and Epistemic uncertainties; (b) identification and bounding/conservative treatment of Intangibles and Splinters; that is of epistemic uncertainties (in parameters and scenarios respectively) that are beyond the reach of any reasonably verifiable quantification; and (c) the use of external experts in a review, rather than in a primary quantification capacity (Theofanous, 2003).

Under the auspices of the US NRC, so-resolved issues include: "Mark-I Liner Attack" (Theofanous et al, 1991), "Direct Containment Heating for PWRs" (Pilch, Yan and Theofanous, 1994), and, in a preliminary rendition, "Alpha Mode Failure for PWRs" (Theofanous et al, 1987). Under support from the US DOE's ARSAP program, the innovative In-Vessel Retention (IVR) technology for Westinghouse's AP-600 and AP-1000 designs was developed and assessed (Theofanous et al 1996; Theofanous et al., 1998; Scobel, Theofanous and Sorrell, 1998), as was an early version of severe accident treatment for GE's SBWR (Theofanous, 1993). The present treatment for ESBWR is based on the same philosophy of approach, same overall methodology, and it is leveraged on ideas, data, and tools developed during all this past work.

The principal consideration in addressing ex-vessel behavior is whether the lower head fails with the RPV being at high or low pressure (HP vs. LP). The demarcation is defined by the capacity of the resulting (superheated steam) blowdown to disperse previously ejected debris into the upper drywell (UDW), and conservatively we will take this here to be at 1 MPa (150 psi) (see Section 21.3.). Thus, as a simplified overview, we have the frame in which two potential containment threatening events will manifest themselves: direct containment heating (DCH) for HP scenarios, and ex-vessel explosions (EVE) for LP sequences. Since both cases lead to large quantities of core debris relocated on the LDW floor, corium-concrete interactions, non-condensable gas generation, and base-mat melt penetration (BMP); that is, long term coolability is an all-pervasive issue.

A quantitative perspective on these matters, as derived from the Level 1 PRA, is shown in Figure 21.2-1. The intent is to illustrate how the CDF is attributed to various kinds of SA sequences, along with the kind of containment integrity considerations appropriate to each case. First we note that, by far, the main contributors to CDF are the Class I (LP) accidents. Class II represents accidents in which core damage could occur in the very long term (>72 hours), and are recoverable by manual actions. These accidents are treated in Level-2/3 PRA. In Class IV we have ATWS scenarios, 71% of which are recoverable at a point of core damage that is small enough to be stabilizable inside the RPV [not credited in Revisions of Level 1 ESBWR PRA after Revision 1], 27% [99.6%] revert to LP with low water level in the LDW, 1% [0%] to HP with spray available, and another 1% [0%] lead to Containment Bypass (Class V) scenarios. The latter along with the Class-V-initiated scenarios (< 1%) [0.47%], and the 71% [0%] of ATWS, lead to systems-dependent source terms, and as such they are addressed in the Level-2/3 PRA.

Now turning to the related containment threats, we see that DCH is only relevant to Class III accidents, while EVE pertains only to Class I. Of the HP sequences, 78% have no sprays available [use of drywell sprays are not included Revision 2 of the Level 2 ESBWR PRA]. This (~1% [~18%] of the CDF) will constitute the limiting condition for potential violation of UDW liner leak tightness under DCH (thermal loads). Of the LP sequences only ~1% [~10%] have sufficient water in the LDW to be of concern for EVE. This (~1% [7%] of the CDF) will constitute the limiting condition for pedestal, and BiMAC failure under steam explosion loads. Finally, and as illustrated in the figure, the BMP is an all-encompassing issue; accordingly, it is central to our severe accident management strategy (Theofanous and Dinh, 2005).

We will show that under conditions consistent with In-Vessel accident evolutions and Level 1 results, the margins to containment failure by all three mechanisms are very comfortable. In particular, we can expect no corium-concrete interactions, and thus we have no risk-significant concerns for long-term pressurization of the containment atmosphere due to non-condensable gas generation. With the PCCS working, similarly, there are no risk-significant concerns for containment over-pressurization and development of leakage flow paths.

On the other hand containment isolation failure must be addressed, and in addition as noted above, we must address the impact of PCCS and the IC systems failure (to remove decay heat) on containment integrity. These are systems-effects driven (i.e. they depend on the long term availability of water to replenish that lost to vaporization) and as such, they are treated in the Level 2 PRA.

An overall framing of issues considered here in terms of Containment Phenomena Event Trees (CPETs) is given in Figures 21.2-2 and 21.2-3. Quantification of these trees, on the basis of results found in Sections 21.3-21.5, is summarized in Section 21.6, which then feeds to the Level 2 PRA .

The following remarks on these trees provide some pertinent clarifications.

(1) As noted already ex-vessel explosions in the ESBWR are only relevant to LP scenarios. The potential severity of the EVEs is parameterized by the depth of the water pool in the LDW, and the probability split among the three classes of events shown in the CPET is obtained from Level 1 results. In the low water case the questions of pedestal, and BiMAC, damage do not arise. For melt release into deep water pools the uncertainties are too great for a ROAAM quantification, thus both are assumed to fail (see Sections 21.4 and 21.6).

(2) Natural depressurization can occur due to thermal loading of the MSL/SRV lines, in which case we transfer to the LP tree as indicated. As discussed in Section 21.3.4.2 uncertainties do not allow for a reliable quantification, thus this node of the tree is taken to be a splinter.

(3) Except for the energetic containment failure events by EVE, or DCH, all other outcomes transfer to the CSETs of the Level 2 PRA addressing long-term containment over-pressurization by loss of decay heat removal.

(4) Debris coolability is addressed in both the LP and HP trees. Success criteria is decomposed into BiMAC supply, a systems question, and BiMAC function, a physics question. Due to the outstanding importance of ensuring LDW flooding soon after the melt exits the RPV, the systems question is addressed in two diverse ways: (a) an active system whose overall unreliability is set to less than 10^{-3} and (b) a passive deluge system operated by means of releasing bottled-nitrogen pressure by a melt-induced mechanism that responds to a high LDW temperature environment. [The diverse/passive deluge system has been deleted with the implementation of squib-actuated valves in the deluge system as described in ESBWR DCD Tier 2, Subsection 6.3.2.7.]

In each case, in addressing a failure, the ROAAM treatment consists of five basic steps:

a. **Identification of the Key Physics.** This includes the definition of all principal mechanisms, their potential interactions, and order of magnitude estimations that we use in defining an optimal approach for quantifying how loads (thermal and/or mechanical) compare to fragilities (failure behaviors).

b. **Definition of a Probabilistic Framework.** This is to define the model(s) for the overall mechanics of quantifying loads, fragilities, and probabilities of failure. In particular this shows the types of uncertainties involved and the manner in which these uncertainties are bounded in the quantification.

c. **Quantification of Loads.** This goes into the technical details of quantifying loads with the intent of enveloping uncertainties. Also covered are the bases for the models used, and evidence of their verification/validation status.

d. **Quantification of Fragilities.** This addresses failure criteria, and in particular, the intent is to provide a solid quantification of failure incipience (conservatively), and at the other end, of gross failure.

e. **Quantification of Failure Probabilities.** Here we transpose loads against fragilities and we evaluate potential for failure.

Finally, according to established ROAAM procedures, GE contracted 9 SA experts to conduct an independent review of the work reported herein. These reports and the authors' responses are reproduced in Severe Accident Management in Support of the ESBWR Design Certification Document, Theofanous & Co. Inc., Tcl-ROAAM-IIX.

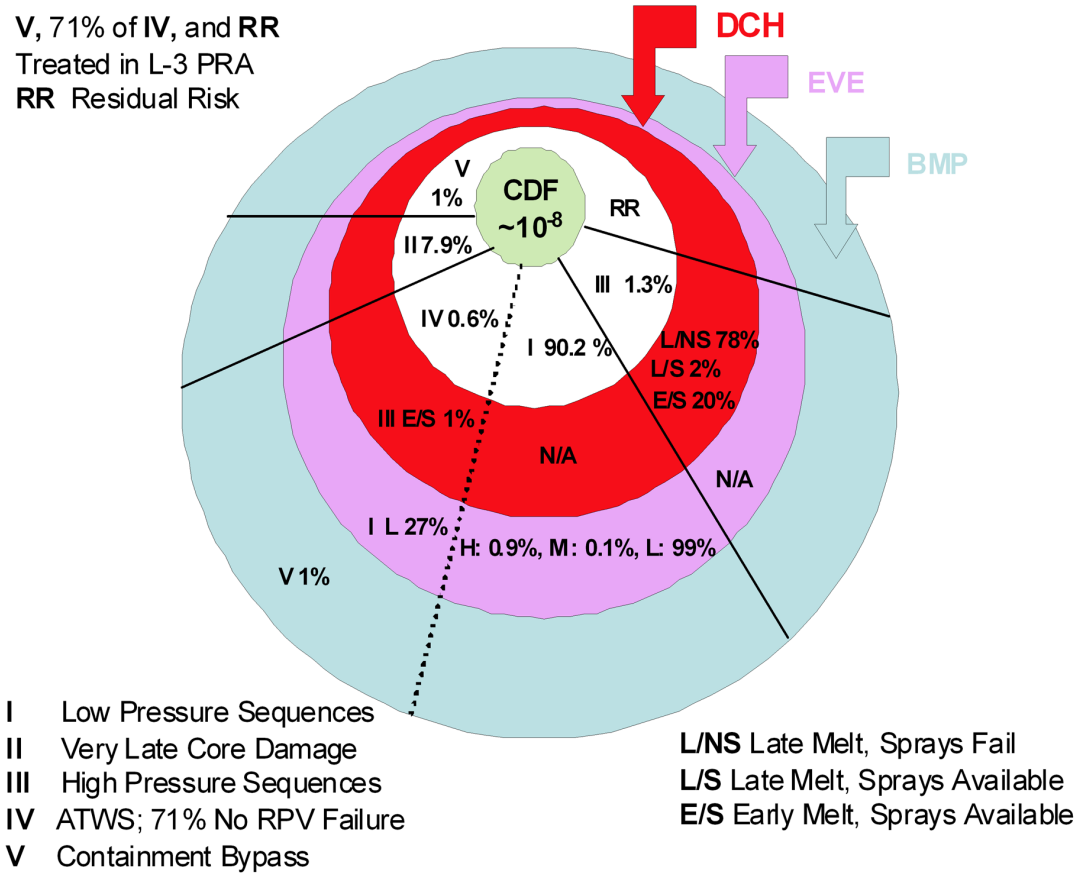

Figure 21.2-1. The Complexion of Severe Accidents in ESBWR

Class II can be ignored—these sequences do not fail the core until after 72 hours and are recoverable with manual actions. L, M and H denote low, medium and high water levels in Lower Drywell, as they are of importance for EVE treatment. See also Figures 21.2-2 and 21.2-3. The EVE is not applicable to Class III because the LDW has only a small amount of condensate in all such sequences. The DCH is not applicable to Class I. The BMP is of concern to all severe accident sequences.

[SEE ADDENDUM 6/2009 AT THE END OF THIS SECTION]

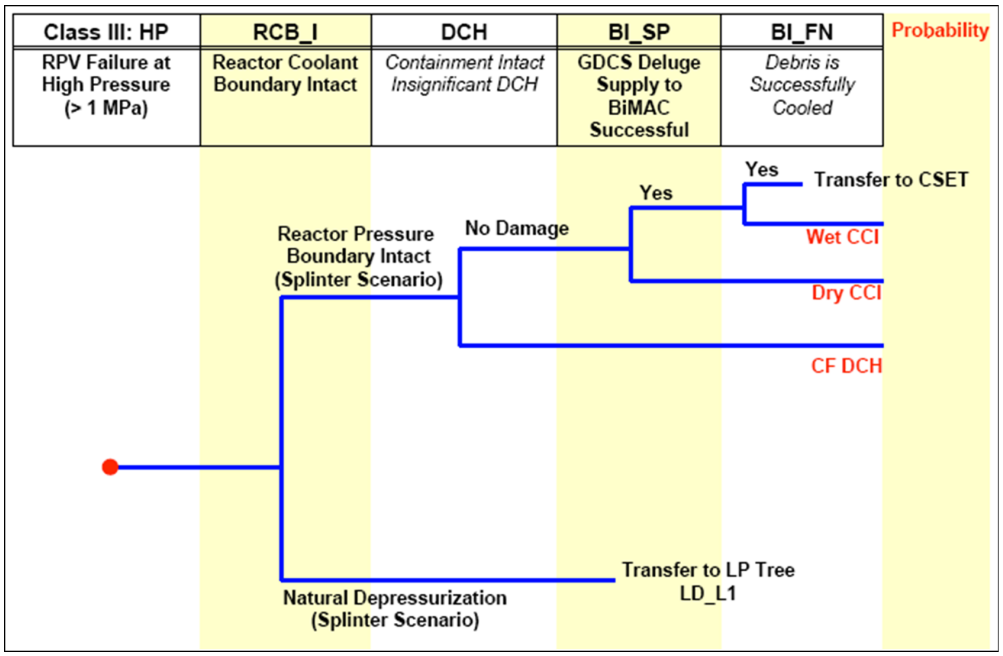

Figure 21.2-2 CPET 1, Key events in ex-vessel high pressure sequences

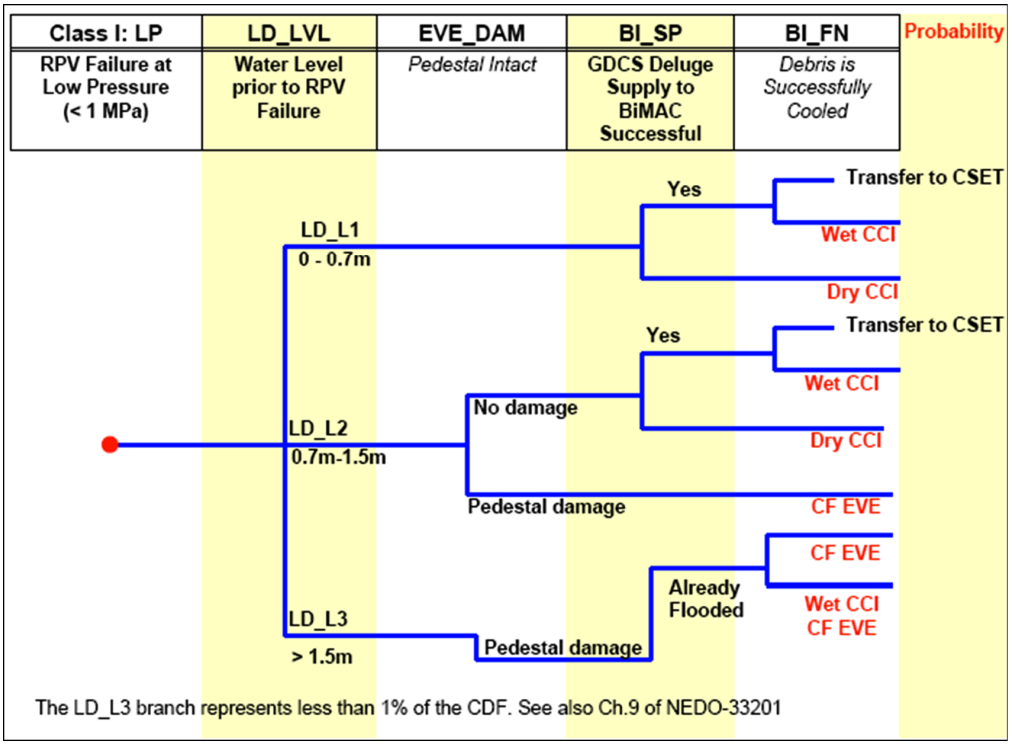

Figure 21.2-3 CPET 2, Key events in ex-vessel low-pressure sequences

21.2.1 References

21.2.-1 GE-NE (2005a), ESBWR Certification Probabilistic Safety Assessment. NEDC-33201P, August 2005.

21.2.-2 GE-NE (2005b), ESBWR Design Control Document, 26A6642BZ Rev.00. August 2005.

21.2.-3 Pilch, M.M., Yan, H. and Theofanous, T.G. (1994), "The Probability of Containment Failure by Direct Containment Heating in Zion," NUREG/CR-6075, SAND93-1535, December 1994. Also in:

21.2.-4 Pilch, M.M., Yan, H. and Theofanous, T.G., "The Probability of Containment Failure by Direct Containment Heating in Zion," Nuclear Engineering & Design, 164 (1996) 1–36.

21.2.-5 Scobel, J.H., Theofanous, T.G., and Sorrell, S.W. (1998), "Application of the Risk Oriented Accident Analysis Methodology (ROAAM) to Severe Accident Management in the AP-600 Advanced Light Water Reactor," Reliability Engineering and Safety Systems, 62 (1998) 51-58.

21.2.-6 Theofanous, T.G., Amarasooriya, W.H., Najafi, B., Abolfadl, M.A., Lucas, G.E. and Rumble, E. (1989) "An Assessment of Steam-Explosion-Induced Containment Failure," NUREG/CR-5030, February 1989. Also in:

21.2.-7 Theofanous, T.G., Najafi, B., and Rumble, E. (1987), "An Assessment of Steam-Explosion-Induced Containment Failure. Part I: Probabilistic Aspects," Nuclear Science and Engineering, 97, 259-281 (1987). M.A. Abolfadl and T.G. Theofanous, "An Assessment of Steam-Explosion-Induced Containment Failure. Part II: Premixing Limits," Nuclear Science and Engineering, 97, 282-295 (1987). W. H. Amarasooriya and T.G. Theofanous, "An Assessment of Steam-Explosion-Induced Containment Failure. Part III: Expansion and Energy Partition," Nuclear Science and Engineering, 97, 296-315 (1987). G.E. Lucas, W.H. Amarasooriya and T.G. Theofanous, "An Assessment of Steam-Explosion-Induced Containment Failure. Part IV: Impact Mechanics, Dissipation and Vessel Head Failure," Nuclear Science and Engineering, 97, 316-326 (1987).

21.2.-8 Theofanous, T.G., Amarasooriya, W.H., Yan, H., and Ratnam, U. (1991), "The Probability of Liner Failure in a Mark-I Containment," NUREG/CR-5423, August 1991. Also in:

21.2.-9 Theofanous, T.G., Yan, H. and Eltawila, F. (1993), "The Probability of Liner Failure in a Mark-I Containment, Part I: Probabilistic Framework and Results," Nuclear Technology 101 No. 3, 299-331, 1993. T.G. Theofanous and H. Yan, "The Probability of Liner Failure in a Mark-I Containment, Part II: Melt Release and Spreading Phenomena," Nuclear Technology 101 No. 3, 332-353, 1993. 49. W.H. Amarasooriya, H. Yan, U. Ratnam and T.G. Theofanous, "The Probability of Liner Failure in a Mark-I Containment, Part III: Corium-Contrete Interactions and Liner Attack Phenomena," Nuclear Technology 101 No. 3, 354-384, 1993.

21.2.-10 Theofanous, T.G., Yan, H./UCSB; M.Z. Podowski, C.S. Cho/RPI; D.A. Powers, T.J. Heames/SNL; J.J. Sienicki, C.C. Chu, B.W. Spencer/ANL; J.C. Castro, Y.R.

Rashid, R.A. Dameron, J.S. Maxwell, D.A. Powers/ANATECH (1993), "The Probability of Mark-I Containment Failure by Melt-Attack of the Liner," NUREG/CR-6025, November 1993.

21.2.-11 Theofanous, T.G. (1993) "Ex-Vessel Coolability for the SBWR", Report to DOE/ARSAP (ANL). August 5, 1993.

21.2.-12 Theofanous, T.G. (1996), "On the Proper Formulation of Safety Goals and Assessment of Safety Margins for Rare and High-Consequence Hazards," Reliability Engineering & Systems Safety, 54 (1996) 243–257.

21.2.-13 Theofanous, T.G. (2003), "Risk Assessment and Management," Ch.19 in Vol.1 in "Comprehensive Structural Integrity", 10-Volume Handbook, Eds. I. Milne, R.O. Ritchie, B. Karihaloo, Elsevier.

21.2.-14 Theofanous, T.G., Liu, C., Additon, S., Angelini, S., Kymalainen O., and Salmassi, T. (1996), "In-Vessel Coolability and Retention of a Core Melt," DOE/ID-10460, Vols. 1 and 2, October 1996. Also in:

21.2.-15 Theofanous, T.G., Liu, C., Additon, S., Angelini, S., Kymalainen O., and Salmassi, T. "In-Vessel Coolability and Retention of a Core Melt," Nuclear Engineering & Design, 169 (1997) 1–48.

21.2.-16 Theofanous T.G., and Syri, S., "The Coolability Limits of a Reactor Pressure Vessel Lower Head," Nuclear Engineering & Design 169 (1997) 59–76.

21.2.-17 Theofanous, T.G. and Dinh, T.N., "Basemat-Internal Melt Arrest and Coolability (BiMAC) device". Patent Application. TcI/GE Document. GE Nuclear Energy. San Jose, March 30, 2005.

21.2.-18 Theofanous T.G., and Dinh, T.N., "Severe Accident Management in Support of the ESBWR Design Certification Document," Theofanous & Co. Inc. Tcl-ROAAM-IIX, May 6, 2007.

ADDENDUM
6/2009: Rev 4 PRA RESULTS

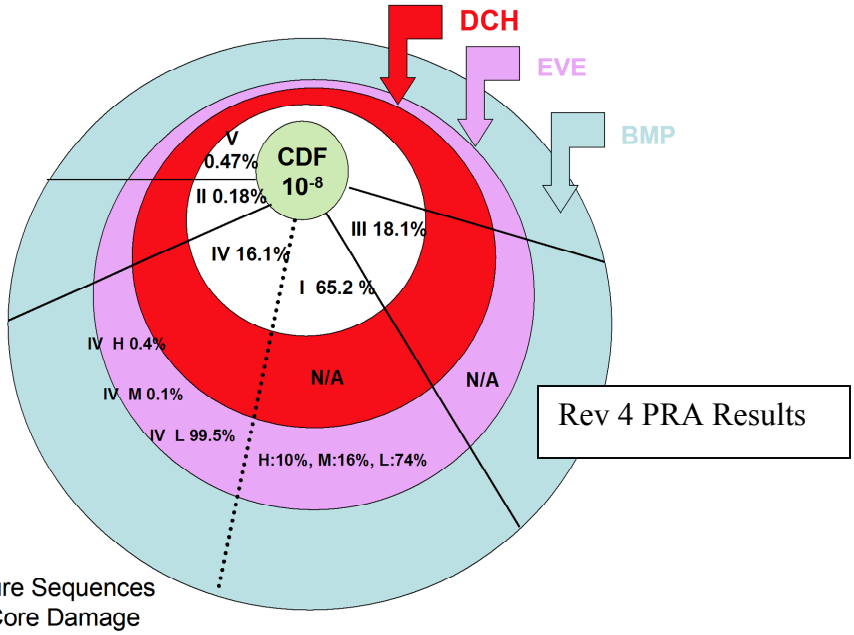

I Low Pressure Sequences
II Very Late Core Damage
III High Pressure Sequences
IV ATWS
V Containment Bypass

Rev 4 PRA Results

Original PRA Results

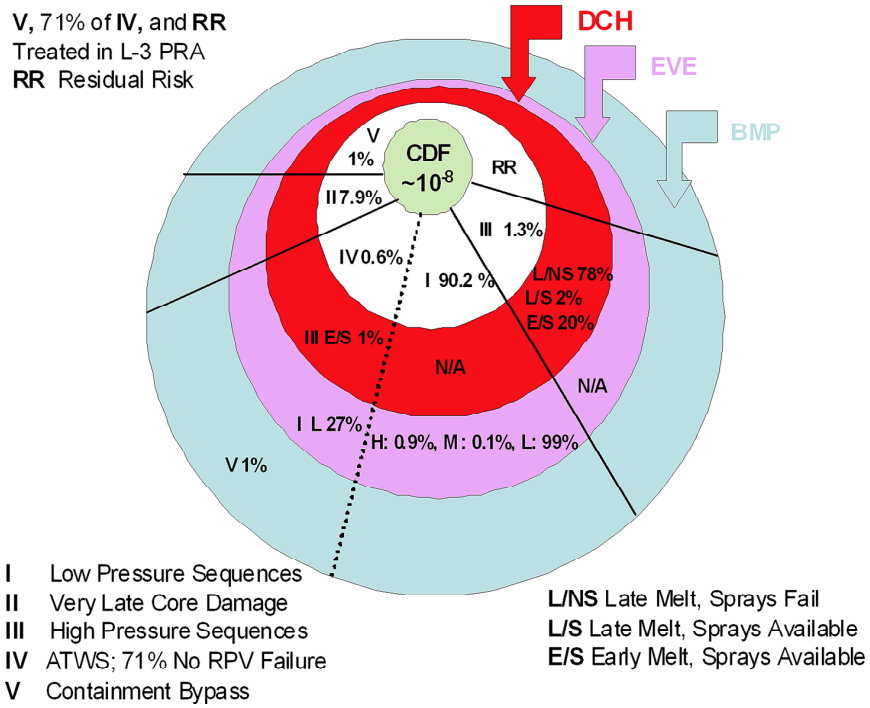

Original PRA Results

It can be seen by comparing the above that refined calculations of Level I PRA yield the same CDF, but with the class I contribution redistributed among classes III and IV to a significant extent. The impact of such changes on SA treatment is negligible. In particular the contribution of high-water level class I scenarios changes from ~0.8% to ~7%.

21.3 CONTAINMENT PERFORMANCE AGAINST DIRECT CONTAINMENT HEATING (DCH)

21.3.1 Overall Considerations

The set of potential accidents that lead to DCH consists of those involving core degradation and vessel failure at high primary system pressure. A necessary condition for this is that a minimum of 2 out the 4 isolation condensers have failed due to either water depletion on the secondary side, or due to failure to open the condensate return valves that keep these IC's isolated during normal operation. In addition, all 8 of the squib activated, reactor depressurization valves, the DPVs, and all 10 of the Safety Relief Valves, the ADS SRVs, must fail to operate. The probability of such combinations of events is assessed at ~2.8 10^{-9} per year [~2 10^{-8} per year], and accordingly, for the ESBWR, such events must be thought of as *remote and speculative; that is, they could, without further ado, be left in the category of residual risks* (Theofanous, 1996, Scobel, Theofanous, and Sorrell, 1998). This is also reflected by the Level-1 PRA results that show HP accidents to constitute ~1% [~18%] of the CDF. Moreover, as in PWR HP scenarios (Pilch, Yan, and Theofanous, 1994), natural convection, and forced flow due to SRV lifting, could be sufficient to thermally load the relief lines to failure, thus producing "natural depressurization", and transition to Low Pressure (LP) scenario (prior to lower head breech by the relocated molten core debris). Still, due to its potentially severe consequences, we chose to examine the likelihood for energetic containment failure due to DCH, and we will show that such a failure is *physically unreasonable*.

The key ingredient towards such a conclusion is that ~14 m^2 (150 ft^2) of vent area, connecting to the enormous condensation potential of the suppression pool, makes it virtually impossible to pressurize the drywell volume. Just as in a LOCA-action of this venting, the timing of "vent clearing" is of essence, and we will pay special attention to modeling it with a high degree of fidelity.

Further, we also examine the potential for liner failure due to the associated high temperatures in the drywell. For the UDW liner this type of failure too was found to be *physically unreasonable*, while for the LDW, due to the immediate proximity and contact with large quantities of melt (given a HPME), local failures, although highly unlikely, cannot be excluded. As explained in the next section, the consequences of such a possibility would be limited due to a standard design feature which compartmentalizes the liner and isolates the gap space of the LDW from that of the UDW so as to clearly eliminate any flow paths to the outside.

21.3.2 ESBWR Design

An overall illustration of the ESBWR drywell, with highlights on features that impact DCH loading is given in Figure 21.3.2-1. Detailed representations are also provided as follows: (a) the lower drywell geometry, in Figure 21.3.2-2, (b) the vent geometry, in Figure 21.3.2-3, (c) the pathway around the RPV including reflective insulation, in Figure 21.3.2-4, (d) the BiMAC device, in Figure 21.3.2-5. The RPV itself is shown in Figures 21.3.2-6 and 21.3.2-7, which also contain the key details of interest here, including the penetration welds on the lower head (Figure 21.3.2-6), and the MSL, SRV, DPV, and IC lines connecting off the RPV upper plenum (Figure 21.3.2-7). The relevance of each of these features can be summarized as follows:

a. Initially the vents are covered with water, so the DW volume must be considered closed for as long as it would take to force this water out under the action of DCH (addition of gaseous mass and energy) on the UDW atmosphere. For pressurization levels of interest to DW integrity, this vent-clearing time is something under 1 s. As described in Subsection 21.3.4.1, and Appendix B, LOCA being a design-basis event, the data, models and prediction of vent-clearing are on the firmest of grounds.

b. The pathway that connects the LDW to the UDW is an annular space around the RPV with a characteristic dimension of ~ 2 m (7ft). As illustrated, in the LDW region this path is partially occupied by the reflective insulation that surrounds the RPV. Assuming that this rather weak structure will provide minimal resistance to the flow, we will, conservatively, ignore its presence. In the UDW region, the path is between the shield wall and the suppression pool wall. At the level of the suppression pool bottom, the path between LDW and UDW is narrowed by 8 massive blocks on which the RPV is supported. The connecting airspace at its narrowest consists of 8 passages, each of 1.7 m^2 (18 ft^2) area; that is 13.6 m^2 (146 ft^2)of total flow area, or a constriction by ~ 70% of the total annular flow path area.

c. The role of the BiMAC cover plate, in addition to providing a base for workers to walk on, is to trap debris released during high pressure melt ejection, and to provide some degree of separation from the high velocity gas flow during the subsequent blowdown phase. Essentially complete separation, and elimination of DCH, could be achieved if such a plate could be suspended anywhere inside the LDW, allowing the melt to ablate through, but deflecting the majority of the gas flow (our CFD calculations indicate more than 90%) in the upward direction — see inset in Figure 21.3.2-5, but supporting this structure (against the gas-dynamic loads) would be problematic. Employing it as a BiMAC cover, while not as effective, makes the concept practical, as the gas-dynamic loads on either side of this plate come quickly to near equilibrium. It is emphasized that this “trapping” is not essential to the demonstration that DCH is not a risk-significant containment failure mechanism in ESBWR. Rather it is provided as a due-diligence measure, to minimize (but not eliminate) the intensity of the dispersal event itself, and if effective in this role, to reduce the chance of LDW liner failure, which otherwise could not be excluded.

d. Finally referring to Figure 21.3.2-7, the intent is to show the in-vessel natural convection flow paths, basically redistributing heat during the oxidation and degradation phases of a severe accident to the upper vessel internals, and through the top portions of the upper plenum into the various lines that lead to the SRVs, DPVs,

and the IC's. The thermal connection to the former one is by forced convection, through the MSL (due to SRV actuation), while for the two latter ones are by natural convection.

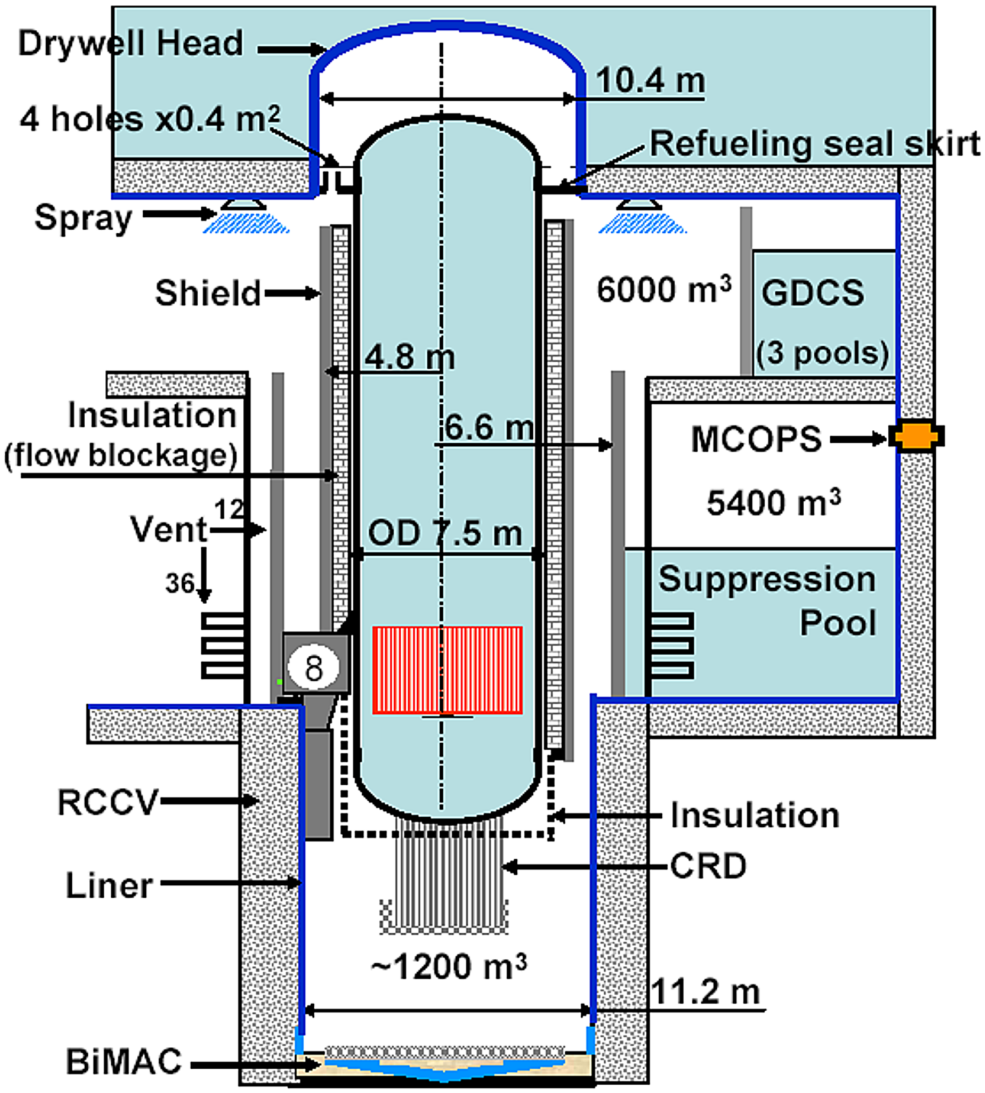

Figure 21.3.2-1 An overall illustration of the ESBWR drywell

An overall illustration of the ESBWR drywell, with highlights on features and scales (volumes) that impact steam/gas flow, melt dispersal and DCH loading. Dimensions and arrangement of important volumes of LDW, UDW and annular airspaces connecting LDW to UDW, and vents to suppression pools are provided to scale. The spray would provide cooling to the drywell atmosphere after a DCH event; however, it is not necessary for reaching the conclusions in this report.

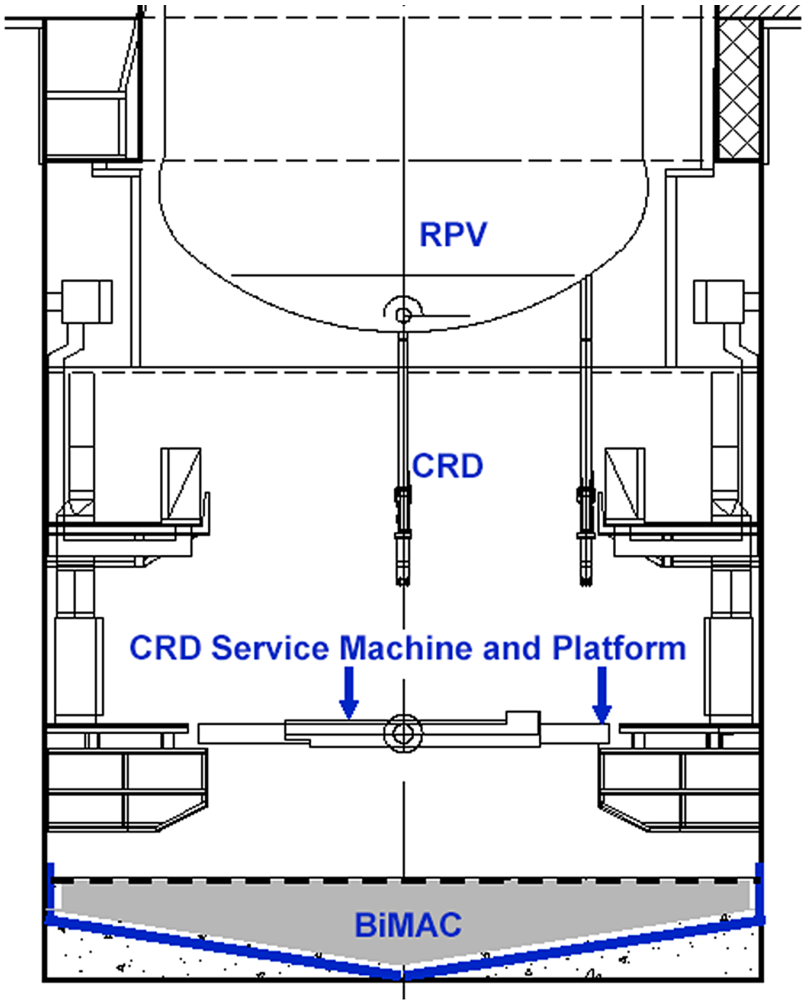

Figure 21.3.2-2 The ESBWR Lower Drywell

The ESBWR lower drywell. The ascending flow of steam and entrained melt along the pedestal wall permeate through CRD service platform and peripheral standing platforms, into the annular space between the vessel and the LDW pedestal wall. The BiMAC is embedded in the layer of concrete (1.5 m height) and is covered by a 0.2 m thick layer of refractory material (ceramic Zirconia). Final design details of the BiMAC will be consistent with Reference 21.5-40.

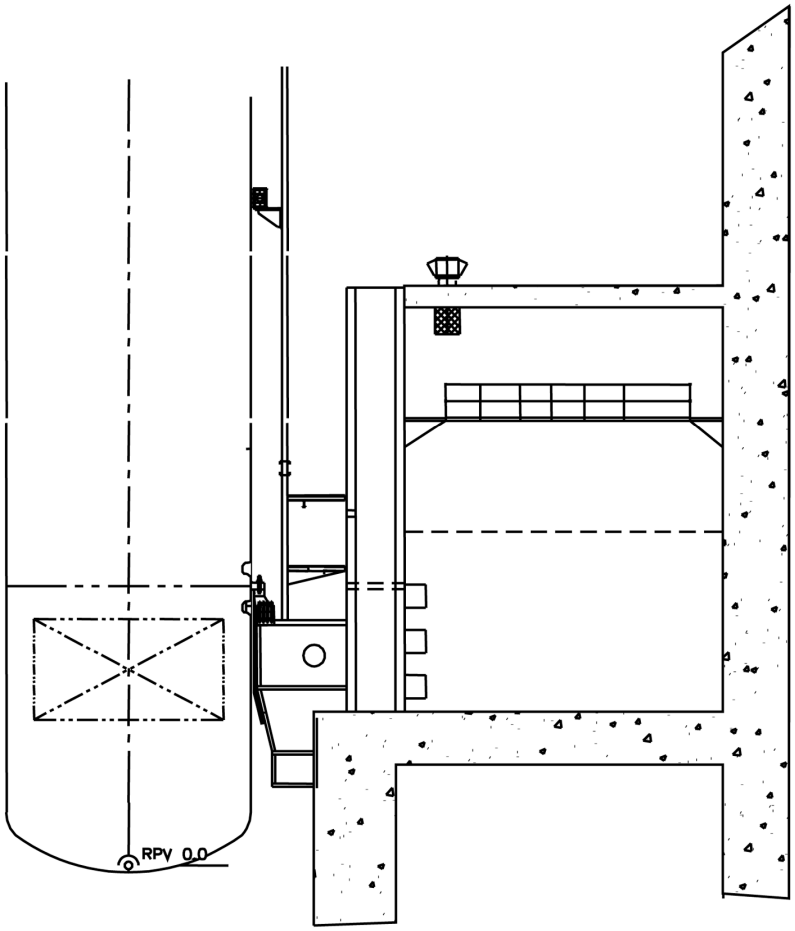

Figure 21.3.2-3.Suppression Pool and Vent Geometry

Suppression pool and vent geometry. There are 12 vertical vents that each feeds a column of three horizontal vents, for a total flow area of ~14 m^2. Each horizontal vent diameter is 0.7 m providing a 0.385 m^2 flow area.

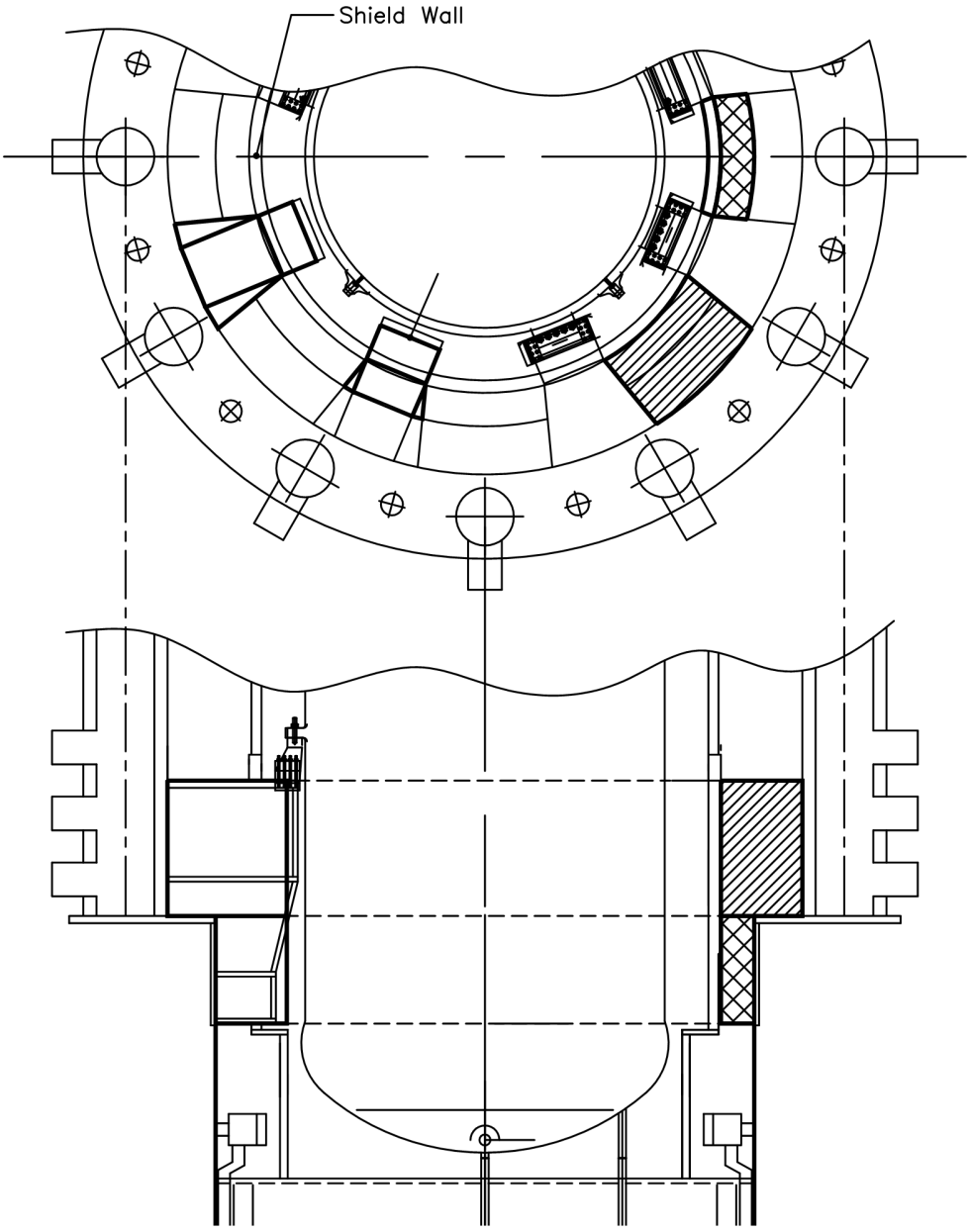

Figure 21.3.2-4.The Pathway Around the RPV

The pathway around the RPV, including reflective insulation and connecting airspace between LDW and UDW. There are 8 blocks on which the RPV is supported. The annular passage (shown by cross-hatched areas) between the shield and the concrete wall is open for airflow. The annular space between the RPV and the shield is filled with insulation materials and presents a flow blockage.

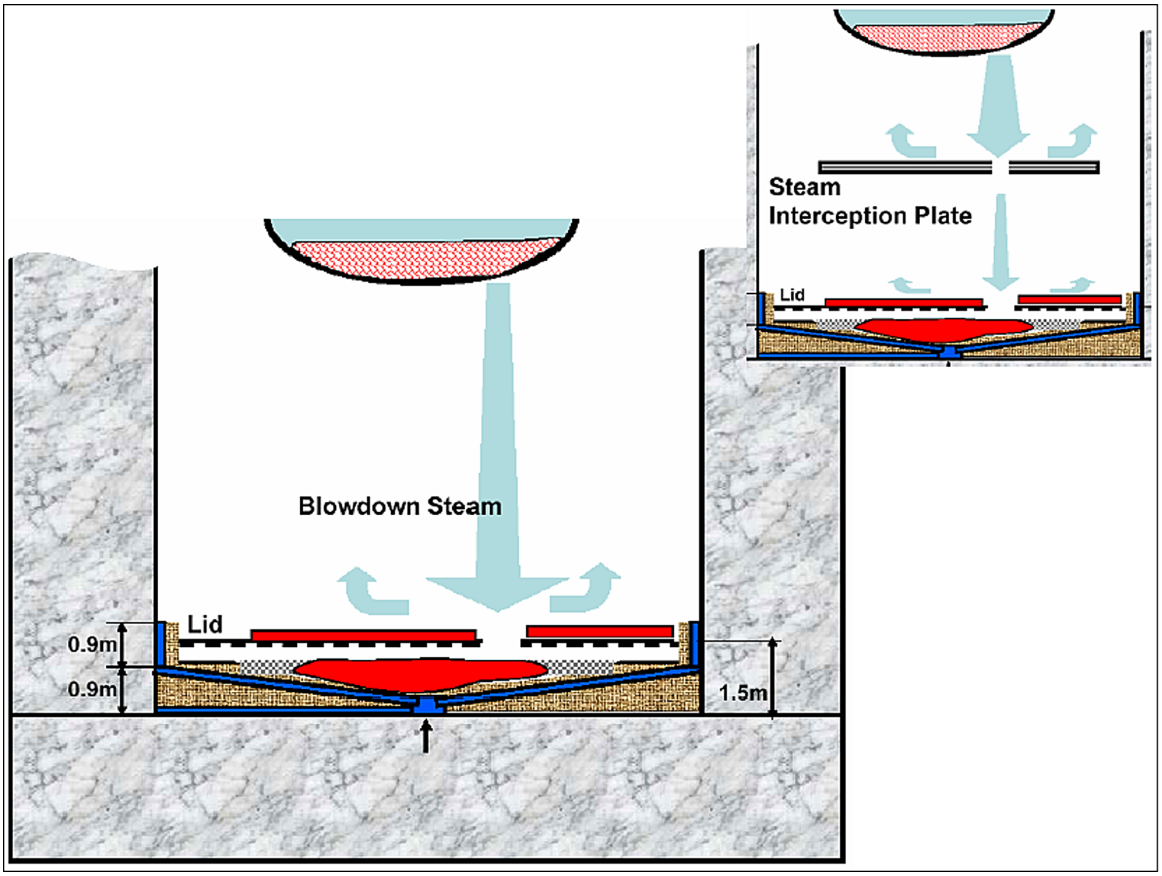

Figure 21.3.2-5.The BiMAC device in the ESBWR Lower Drywell

The BiMAC device and its incorporation in the ESBWR Lower Drywell. The SIP (Steam Interception Plate) concept is shown in the insert.

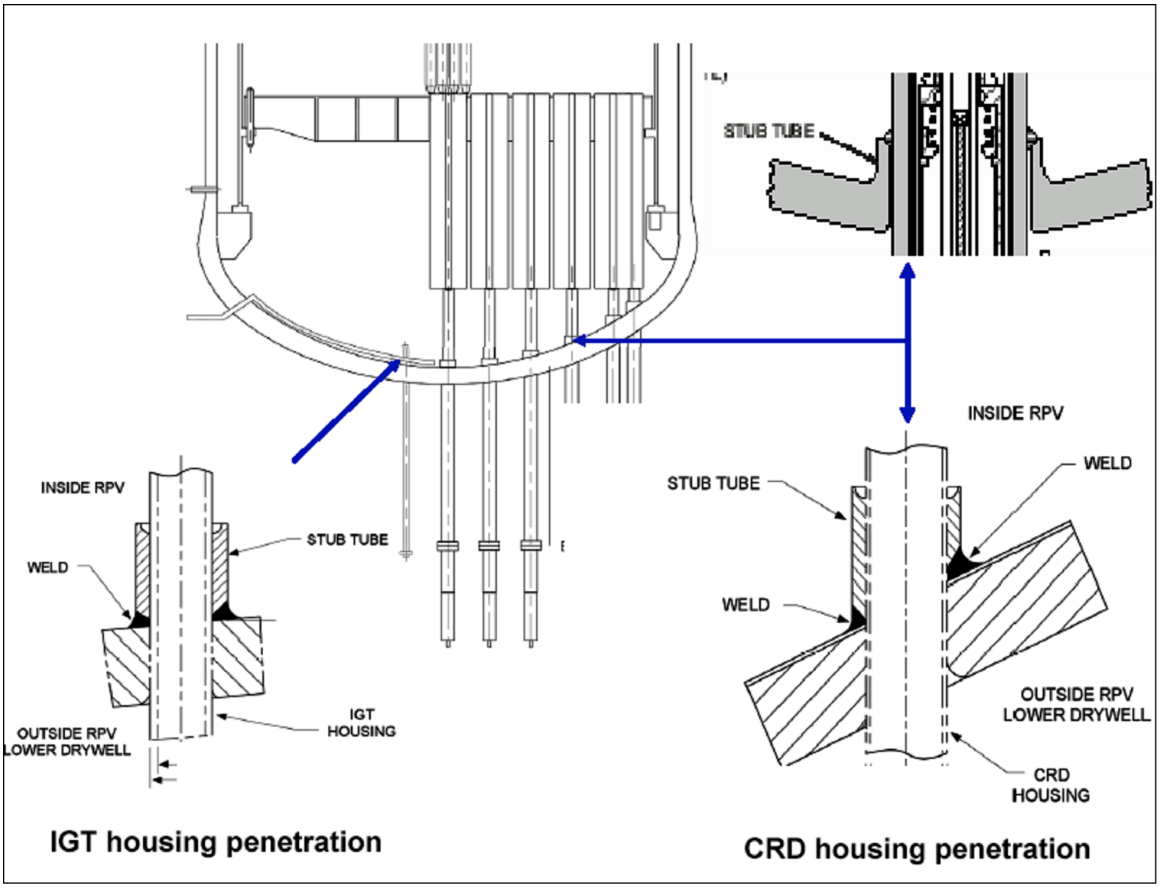

Figure 21.3.2-6.The RPV Geometry (lower part)

The RPV geometry (lower part), including the penetrations and penetration welds on the lower head. The CRD and IGT are supported on the vessel lower head by the weld between the penetration housing and the on-vessel stub tube. The weld elevation is 15 cm from the vessel inner surface. Upon core melt relocation to the lower plenum, a number of CRD and IGT become submerged in the core debris or core melt pool. This can result in vessel failure due to thermal attack on the penetration, failure of the stub-tube-to-penetration weld, and ejection of the penetration.

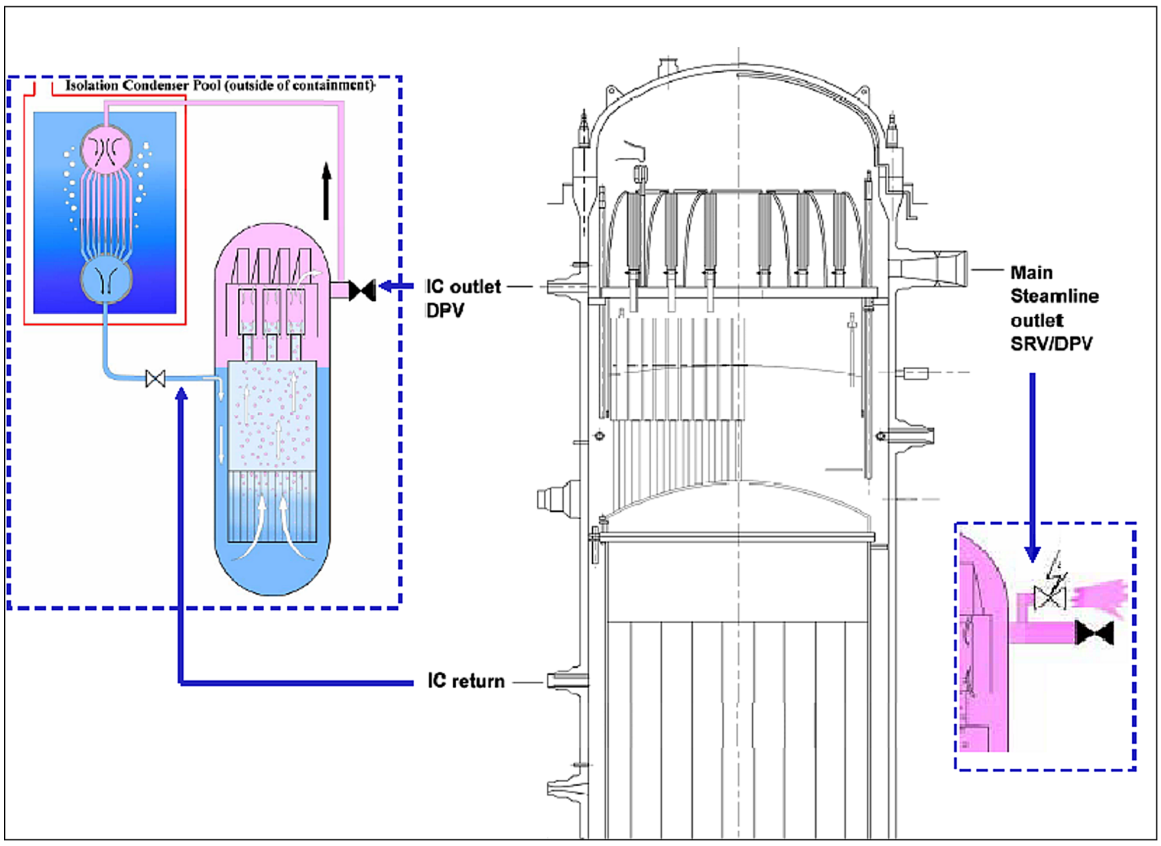

Figure 21.3.2-7. The Upper RPV with SRV, DPV, and IC lines

Intermittent flow of hot gases through SRVs (and into the Main Steam line) would thermally load the lines that constitute the relief path. The thermal connection to the IC lines is by natural convection, and thus weak compared to that of the SRV/MS lines. Also shown, in areas above the core and in the upper plenum, are structures, which present heat sinks for hot gas/steam that, would emanate from a degraded core.

21.3.3 Previous Work

Direct containment heating has been considered to be a major containment integrity issue in PWRs, and this drove very extensive research efforts during the late 80's and early 1990's. These efforts culminated with issue resolution in a ROAAM framework as documented in Pilch, Yan, and Theofanous (1996), and Pilch and Allen (1996). Reviews on the subject have been presented by Pilch et al (1997), and by Pilch and Henry (OECD, 1996). The later considered also the BWR setting and recognized the significant load-mitigating role of venting into the WW heat sink.

The principal ingredient in quantifying DCH loads in this previous work was the realization that oxidation of the reactive components in the melt, and energy transfer to the containment are limited by the entrainment/dispersal process occurring over a time scale that restricts contact to only a fraction of the available (in the RPV) steam. Within this time scale the melt-steam contact was found to be so intense as to be describable by a thermo-chemical-mechanical equilibrium

process. The principal experimental data came from the Integral Effects Tests (IET) (Allen et al., 1994; Binder et al., 1994), conducted for the US NRC with comprehensive review and input on scaling to reactor conditions from a group of experts. The interpretation and application to reactor predictions were made by means of the CLCH model (Yan and Theofanous, 1996) and the two-cell equilibrium model (Pilch, 1996). For PWRs the containment heat sinks played no significant role, and combustion of hydrogen produced in the DCH process had to be addressed. Also, for the PWRs the spontaneous depressurization scenario played an important role in the overall issue resolution scheme. In the ESBWR we need not be concerned about combustion in the containment atmosphere, and we will take no credit for spontaneous depressurization.

These developments were not available in the singular prior licensing assessment of DCH for a BWR. Done for the ABWR (GE, 1987; 1994), it was assumed that 20% of core (molten materials) was dispersed (and equilibrated with the atmosphere) inside the 8,000 m^3 (280,000 ft^3) UDW volume within 2 seconds, and the calculations produced over-pressurization that exceeded the structural capacity of the DW. This unrealistically conservative result was one of three reasons cited by the US NRC (1994) for judging that conditional (given a core melt) containment failure probability for ABWR could be as high as 10%.

21.3.4 Present Assessment

21.3.4.1 Key Physics in DCH

Direct containment heating can be expected when high velocity steam happens to impinge upon melt already released into a containment compartment, thus creating regions of fine scale mixing, large interfacial area for heat transfer, and oxidation of metallic components in the melt. The so-heated steam, flowing at very high volumetric flow rates, provides a mass-and-energy source that can pressurize and heat the receiving atmosphere. Con-currently, the finely atomized melt is carried against gravity into the receiving volume(s), where the steam velocities are highly reduced, and the particles are allowed to fall (de-entrain). In ESBWR the mixing occurs in the LDW, while the main receiving volume, in which de-entrainment occurs, is the UDW—these correspond to the reactor cavity and the sub-compartment(s) of Large Dry Containments (LDC) in PWRs respectively. In distinction to LDCs, in the ESBWR, as in all BWRs, the receiving volume, rather than being closed, is vented to another volume, the WW, which contains a large and effective heat sink. The key physics that drive all these phenomena, and that need to be quantified in predicting a realistic outcome, are as follows:

a. **Natural Depressurization and RPV Lower Head Breach.** Natural depressurization, and thus transition to a LP scenario, would occur if any of the MS, SRV, DPV, or IC lines were to fail (due to thermal loading by gas natural convection) prior to lower head breach (by melt attack). The heat source is the melting/oxidizing reactor core. The heat transfer medium is the steam (and hydrogen) trapped inside the RPV at high pressure, and thus at high density. The process is by natural convection. It is set up between the core region and the cooler upper internal structures whose heat capacity defines the heat-up rates of the gases in the upper plenum. The flow of these gases into the MS, and SRV lines would be convective, as the SRVs lift periodically to relieve pressure, and thus the material temperatures reached would be close to that of the hot gases. As we will see below, the time scale for the melt material to reach the lower plenum in large quantities is ~1 hour, and in this time period gas temperatures reach up

to ~1,000 K (1300 °F). This indicates conditions in the neighborhood of creep rupture (Smith, 1971, Reddy and Ayers, 1982) of the lines involved. In competition with this is a set of complicated processes in the lower plenum that lead up to lower head failure. These include quench and reheating of the relocated core debris, melt attack of lower head penetration welds and RPV failure by ejection of the penetration equipment involved, gradual re-melting of the core debris, and ultimately, if for some reason penetration failures did not occur, heating and creep rupture of the lower head material itself.

b. **Melt Ejection, Vessel Wall Ablation, and BiMAC Refractory Cover Ablation:** Due to negligible resistance by the LDW atmosphere, the melt jet would remain essentially coherent until it hits the LDW floor, and the BiMAC cover plate, which would then be penetrated essentially instantaneously to allow free access to the sacrificial refractory layer that covers and protects the top of the BiMAC pipes. The vessel wall would ablate due to heat transfer from the superheated melt. So would the refractory material if melt temperature exceeds its melting point. These processes are well understood and this understanding is supported by experiments. Results depend on the melt composition and superheat and will be treated in a bounding fashion. Similarly, the amount of melt mass involved in the ejection process, and the mass fractions of Zirconium and Iron in it, are treated in a bounding fashion.

c. **Steam Blowdown:** The steam inside the reactor vessel would expand adiabatically during blowdown, and the steam discharge rate is defined by choked flow at the vessel breach area(s). Both processes can be accurately simulated by means of simple thermodynamics (ideal gas equation of state, adiabatic expansion) and Computational Fluid Dynamics (CFD) simulations respectively. Figure 21.3.4.1-1 shows the gas-dynamic pressures established in the LDW during a typical blowdown from a full-pressure RPV (safety valve set-point). As illustrated, the discharge flow accelerates to form a supersonic jet, with key characteristics of flow area expansion by a factor of ~10, and a loss of stagnation pressure due to repeated spontaneous/internal shock and expansion wave formation by ~75% to 90%. This jet, upon impinging the floor, and then again upon impinging the sidewalls, yields wall jets, which remain largely coherent and maintain velocities of hundreds of meters per second. An idea of the energy involved and of the overall flow pattern developed in the LDW can be obtained from snapshots of the velocity distributions from steam-only flow (no melt) in CFD simulations (Figure 21.3.4.1-2). Importantly, rough treatments that smear the flow out over the whole LDW cross-sectional area, such as those made in a few old attempts to define entrainment limits, would seem to be in error. Rather, momentum flux localization is the essential mechanism that determines melt atomization, and entrainment potential in DCH events for such a geometry.

d. **Interfacial Instability, Breakup, Entrainment, and Carry-over of Melt Exposed to the Gas Stream Inside the LDW.** Liquids exposed to high velocity gas streams atomize and become dispersed. The mode and magnitude of the interfacial instability responsible for this behavior depends on the Weber number, which is the ratio of the destabilizing momentum flux of the gas (ρv^2) to the stabilizing surface tension force (▪ /R). For corium melts, the surface tension is about 10 times that of water, so the stability limit will be (for the same momentum flux) at a length scale that is ~10 times

that of water. For example at a gas velocity of 300 m/s (980 ft/s)and atmospheric density of 1 kg/m^3 (6E-2 lbm/ft^3), the stable droplet size for water is ~10 microns, while for corium it is ~100 microns. This stability limit is captured by a critical Weber number of ~10. Thus even a relatively small drop of 10 mm (0.4 in) will experience an initial We number of 10^3 and a breakup pattern such as that illustrated in Figure 21.3.4.1-3, except that the mist shown would be at length scales of ~100 rather than ~10 microns.

Melt particles of 100 microns size can be suspended by air/steam velocities of as low as ~ 5 m/s (16 ft/s). This is to be seen in the perspective of the jetting velocities seen in Figure 21.3.4.1-2, and some ~10's of m/s exiting the lower drywell under typical high pressure steam blowdown rates. In addition, macroscopic motions are induced by pressure forces that accelerate bigger masses of liquid up the pedestal walls, in the manner illustrated (for a geometrically-scaled ESBWR geometry) in Figure 21.3.4.1-4. There is no question that any exposed melt inside the LDW will be atomized and dispersed into the UDW. Much of it would then be carried into the suppression pool, while some fraction would de-entrain and deposit on the UDW walls or fall on the floor, in a highly dispersed state. As discussed in Subsection 21.3.4.3, we can estimate the dispersal rates in terms of the DCH-scale as determined from scaled experiments (the IET series of tests).

e. **Entrainment of Melt Captured inside the BiMAC.** The geometry of concern is illustrated in Figure 21.3.4.1-5. While the pressure established inside the BiMAC is the same as the stagnation pressure on the top of the cover plate, due to high frequency flow fluctuations, these pressures are unsteady, and as we found in scoping experiments, a net circulation pattern is established that continuously brings liquid into the immediate vicinity of the opening from where it is entrained to the outside in a highly atomized form. The velocities in this region can be as high as 600 m/s (2000 ft/s), and the mass loading on the flow is rather low (that is, we have a metering effect, defined by the internal circulation rate of the melt, on release and dispersal due to the BiMAC), so the Weber numbers may approach 10^4 and the length scales of atomization may be as low as 10 micron. Such particles could be carried around by gas flows as low as 2 m/s (7 ft/s).

The influence of water (preexisting in the LDW) in any of the above does not need to be considered because the only HP scenario that can lead to flooded LDW is the SBLOCA with loss of DPV/SRV action and CRD water supply, having a core damage frequency of ~$7x10^{-13}$ [~$3.2x10^{-10}$] or 0.01% [1.9%] of the total CDF.

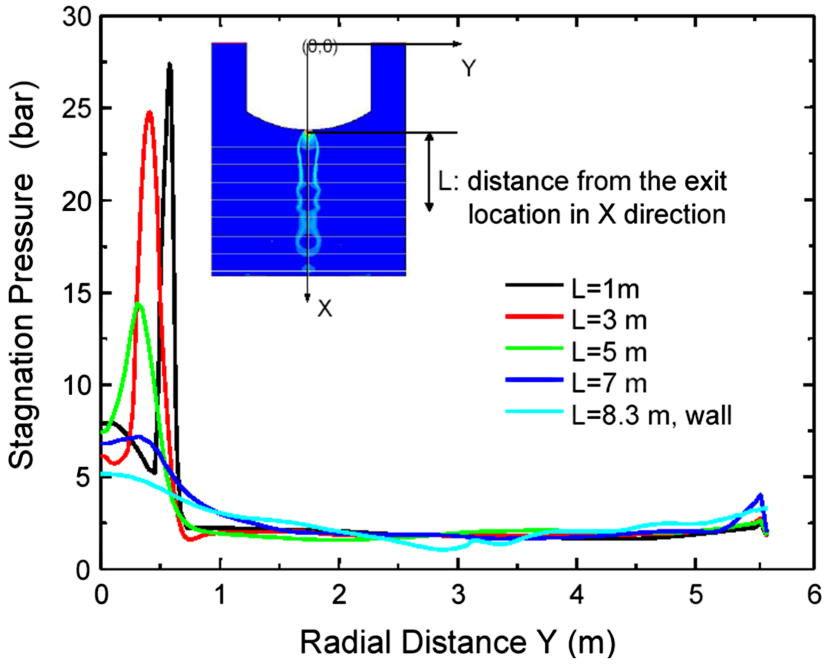

Figure 21.3.4.1-1. The Stagnation Pressures in the LDW

The stagnation pressures (PS + $rV^2/2$) in the LDW (t ~ 188 ms) during a typical blowdown from a fully pressurized RPV through a 0.40 m in diameter hole.

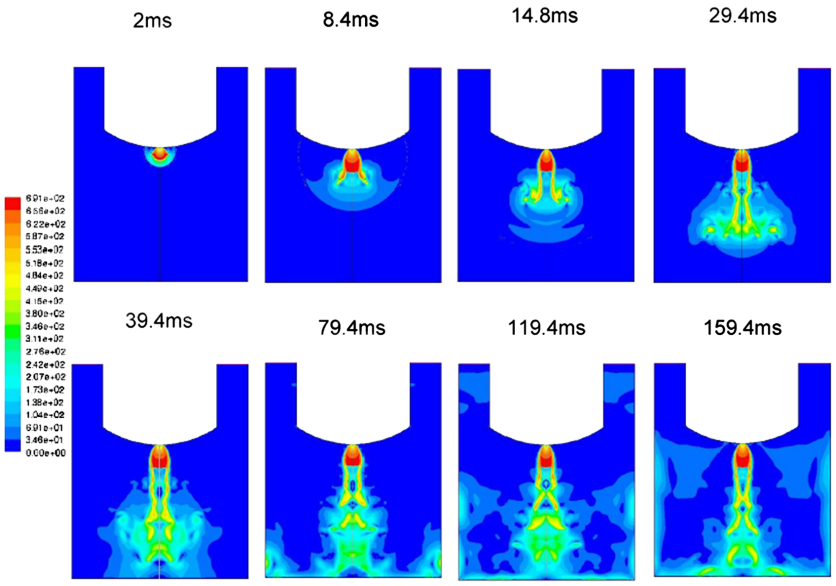

Figure 21.3.4.1-2. Velocity Distributions in the LDW From Steam-Only Flow

Velocity distributions in the LDW from steam-only flow (no melt) in CFD simulations. The velocity scale is shown on the left. The maximum value ~ 700 m/s.

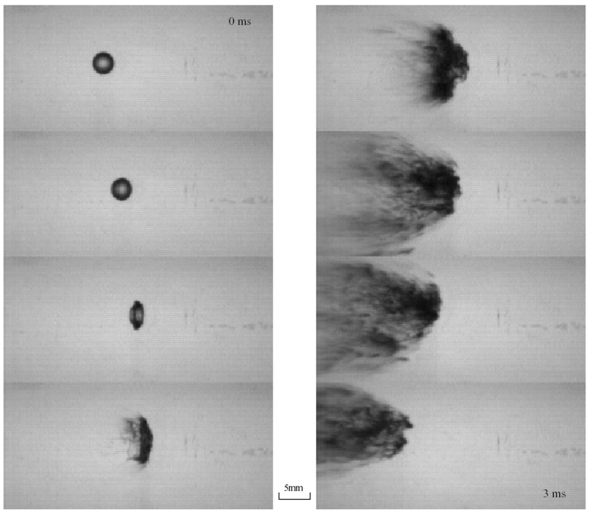

Figure 21.3.4.1-3a. Water Drop Breakup at We ~ 10^3

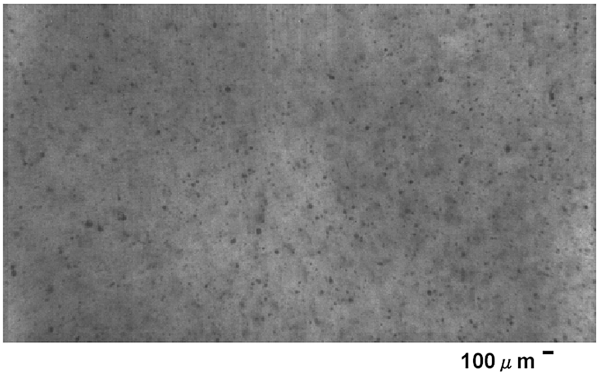

Figure 21.3.4.1-3b. Close Up Image Of Fragments From A Breakup at We ~ 10^3

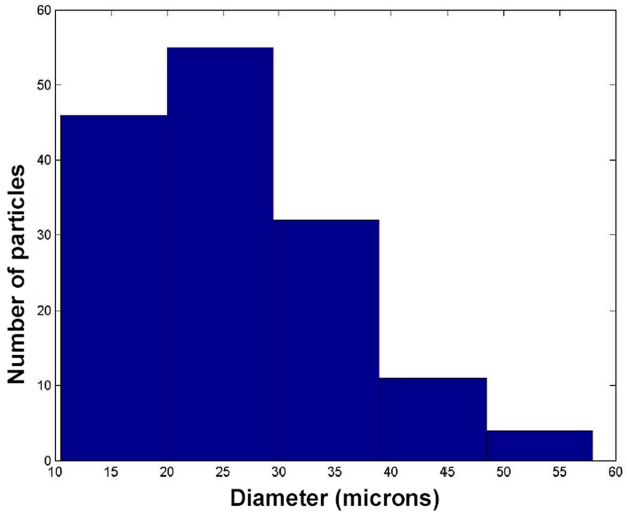

Figure 21.3.4.1-3c. Droplet Size Distribution in Figure 21.3.4.1-3b.

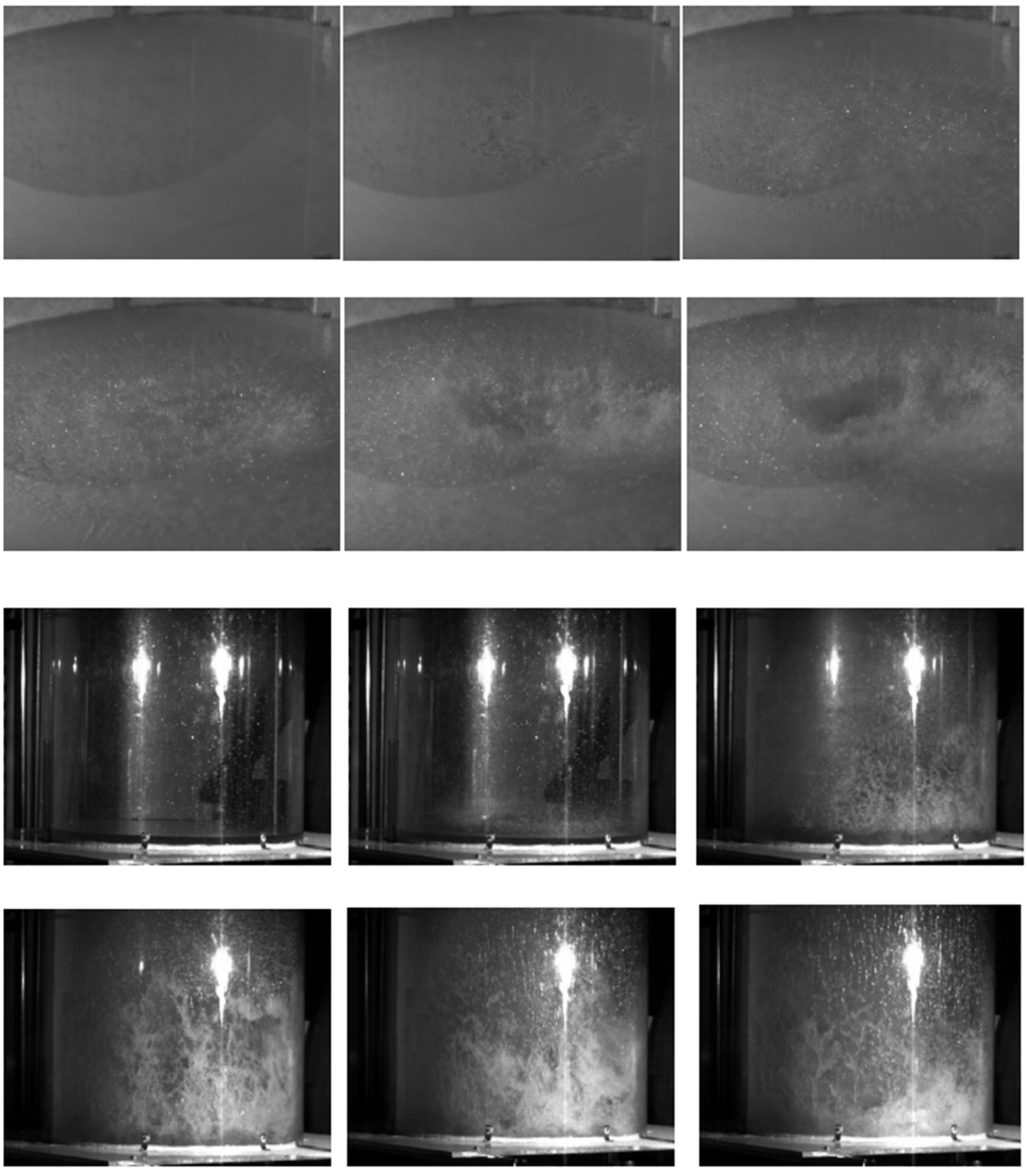

Figure 21.3.4.1-4. Liquid Flow and Entrainment During Gas Blowdown

Visualization of liquid flow and entrainment during gas blowdown from 1 MPa pressure into a 1/10 scale model of the ESBWR LDW. Upper 6 frames: Close-up view of the gas jet interacting with liquid layer resting on the vessel bottom plate. One can see the general pattern of interfacial instabilities, liquid atomization, and entrainment. Lower 6 frames: Far view of the liquid dispersal and carry-over with the gas flow. The blowdown gas impinges upon the liquid, then spreads radially towards the cylinder boundary, and ascends as wall jets along the pedestal wall, carrying the liquid with it.

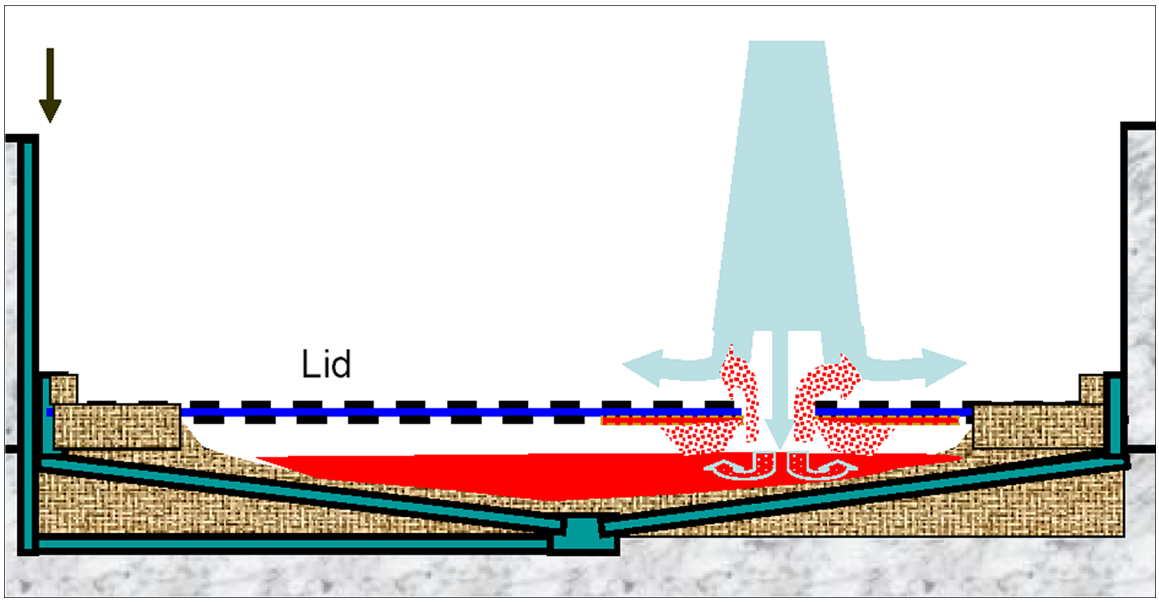

Figure 21.3.4.1-5. Conceptual Visualization of Melt Entrapment in BiMAC

Conceptual visualization of melt entrapment in BiMAC and subsequent gradual entrainment (blowdown steam in blue and melt/debris in red).

21.3.4.2 Probabilistic Framework

First we address spontaneous depressurization. The precipitous loss of strength of the RCS wall/piping material at temperatures above 700 K (800 °F) is illustrated in Figure 21.3.4.2-1. The relevant stress levels in various piping components are listed in Table 21.3.4.2-1, and shown also in Figure 21.3.4.2-1. We can see that all these piping components are at risk of failure once they reach temperatures over ~1,000 K (1300 °F), and that due to the stress levels involved such a failure would be far more likely to occur in the MSL. In fact, such temperature levels are known to be typical of the heat-up found in high pressure scenarios. For example, as noted already, MAAP calculations for the ESBWR show peak temperatures of ~900 K (1200 °F) (GE-NE, 2005a). Moreover, in the DCH issue-resolution work for PWRs (Pilch et al, 1996), calculations with SCDAP/RELAP (at 8 MPa, 1200 psi) show temperature levels reaching up to 1,700 K (2600 °F).

Table 21.3.4.2-1
Stress levels in piping components
Vulnerable to heating-up during core degradation at high pressure (evaluated for PRCS ~ 8 MPa, 1200 psi)

Component	**Diameter D, m (in)**	**Thickness δ, m (in)**	**Hoop Stress, MPa (psi)** $S = P_{RCS}.D/2\delta$
SRV Inlet Line	0.17 (6.7)	0.050 (2.0)	13.6 (1970)
IC Inlet Line	0.45 18)	0.080 (3.1)	22.5 (3260)
MSL (before SRV)	0.70 (28)	0.037 (1.5)	75.7 (11000)

We can see that for the MSL we are clearly in the creep rupture region. However, considering the uncertainties involved in calculating these temperatures, and the sensitivity of material properties in this temperature region, we believe that this aspect of HP scenario transition to LP should be treated as a splinter at this time. In practical terms this means that we take no credit for spontaneous depressurization. However, we do note that high pressure sequences that lead to high pressure melt ejection may not be physically possible for the ESBWR.

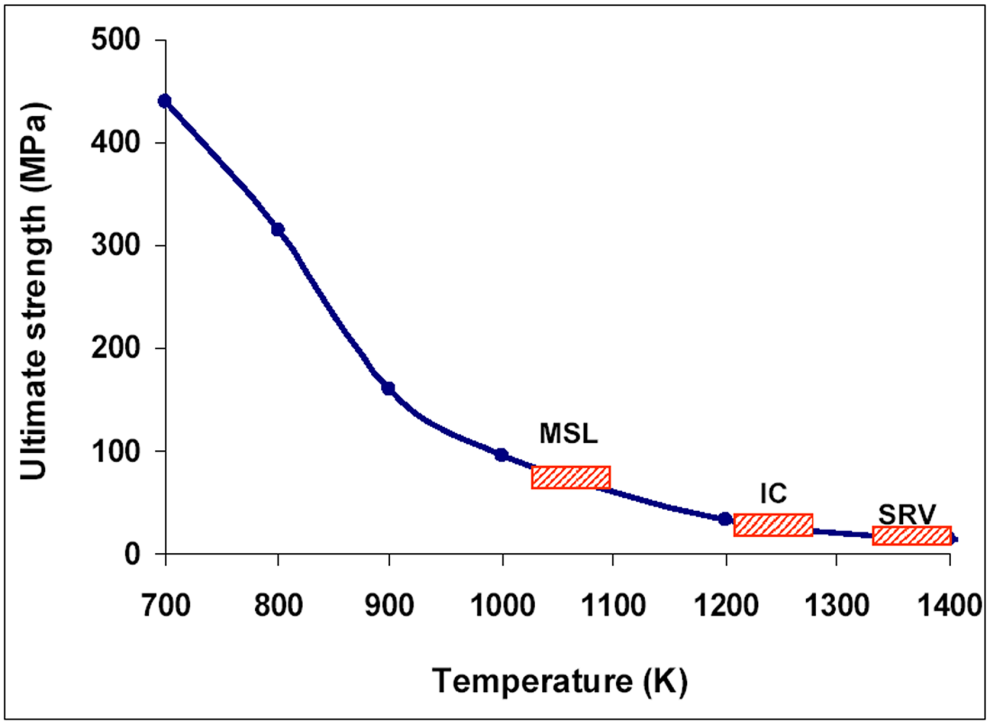

Figure 21.3.4.2-1. Ultimate Strength of Steel in the High Temperature Range

Ultimate strength of steel in the high temperature range. Also shown are the relevant temperature levels for creep rupture of the MS, IC, and SRV lines.

Turning now to DCH loads, our principal concern is to address energetic failure due to DW over-pressurization. Our approach evolved, as we came to understand and appreciate the interesting dynamics of such a system, gradually and through various kinds of calculations. As it turns out there are three different kinds of pressurization regimes that are possible to realize, depending primarily on the size of the vessel breach area. One regime was found in trying to illustrate the case of pressurization levels approaching the failure pressure of the containment (1.2 MPaG (170 psig) –see section 21.3.4.4) given an arbitrarily large breach area (>1 m (3 ft) in diameter). As expected this case involves extremely fast dynamics that tie closely to the clearing and the flow capacity of the vents. The second regime obtains for break areas at the upper end of credible creep ruptures (~0.5 m (20 in) in diameter) as determined in the PWR DCH issue-resolution documents (Pilch, Yan, and Theofanous, 1996, and Pilch and Allen, 1996). This regime exhibits intermediate dynamics, with pressurization levels reaching up to only half of the 1.2 MPaG (170

psig) needed for approach to failure. Finally the third regime, found for break areas that correspond to a single penetration failure (after ablation to ~0.2 to 0.3 m (8 to 12 in) in diameter), is quasi static, exhibiting very low pressurization levels that depend mainly on the amounts of Zirconium available to react. The hypothetical case (first regime) is considered in this section as a way of providing perspectives on the bounding load calculations, including the other two regimes, which are presented in the next section. These calculations will also yield a way for bounding the UDW atmosphere temperatures as needed for the less important, yet still interesting question of creep-induced liner failure.

A hypothetical case that yields the first regime (see Subsection 21.3.4.3 for the mathematical model used in capturing them) is illustrated in Figure 21.3.4.2-2. The condition represented is for 300 metric tons (330 tons) of melt, containing 60 metric tons (66 tons) of Zirconium (20% content in the melt), it being dispersed by the blowdown from a vessel breech equivalent to a hole 1 m (3 ft) in diameter. The melt entrainment time is taken as 1 s, the blowdown time constant is ~1 s, thus implying a DCH-scale of ~1. This means there are no significant mitigative effects due to melt-steam incoherence. The peak pressure that develops in the LDW is due to the rapid energy supply by the DCH phenomenon, taken at an extreme manifestation here for purposes of illustration. At around 0.2 s, the pressurization due to this energy supply rate is compensated by mass/energy loss to the UDW, leading to a drop in pressure, till at ~0.4 s the balance again shifts in favor of supply, thus yielding a second pressure rise transient. By this time the LDW and UDW behave in tandem, until the end of melt dispersal, at which time the peak pressure of ~1.2 MPa (170 psia) is reached. Vent clearing occurs in the 0.4 to 0.6 time interval, and the effect is seen to moderate the rate of pressure rise. Throughout this extremely fast transient the WW pressure has been hardly affected, while the magnitude of the second pressure peak is controlled by the flow capacity of the vents. Further in Figure 21.3.4.2-2 we see that the end of dispersal is followed by a rapid cooldown period, as the expanded, “cool” steam washes away the hot gases from the LDW. Increasing the DCH time scale to 2 or 3, that is melt entrainment times of 2 or 3 s respectively, has no significant effect on all these features of the transient. This is because the DCH contact process is already saturated (Yan and Theofanous, 1996), and the maximum possible extent of oxidation has taken place. From this bounding (in RPV pressure and amounts of melt and Zirconium) condition, the only way to effect a higher dynamic pressure would be by increasing the breach area even further, but this is already 4 times the upper bound considered credible in creep rupture scenarios for PWRs (Pilch, Yan, and Theofanous, 1996, and Pilch and Allen, 1996), and more than ~10 times that created from a single penetration failure due to ablation from a 300-metric tons (330 tons) melt (see Subsection 21.3.4.3). Further, in the case considered above we use the total quantity of Zirconium in the core, which for the ESBWR is 76 metric tons (84 tons), minus the 16 metric tons (18 tons) taken to have been already reacted to produce a containment pressure of 0.25 MPa (36 psia) consistently with that assumed to be initially present.

Thus it is clear that overpressure failure of the ESBWR DW due to DCH is physically unreasonable. Moreover, it is clear that this conclusion is robust in that it does not depend on a host of (intangible) parameters that previous (PWR) assessments were found to depend on, such as, the total quantity of the melt involved and its Zirconium content, the breach area, and combustion in the receiving atmosphere (see Figure 21.3.4.2-3).

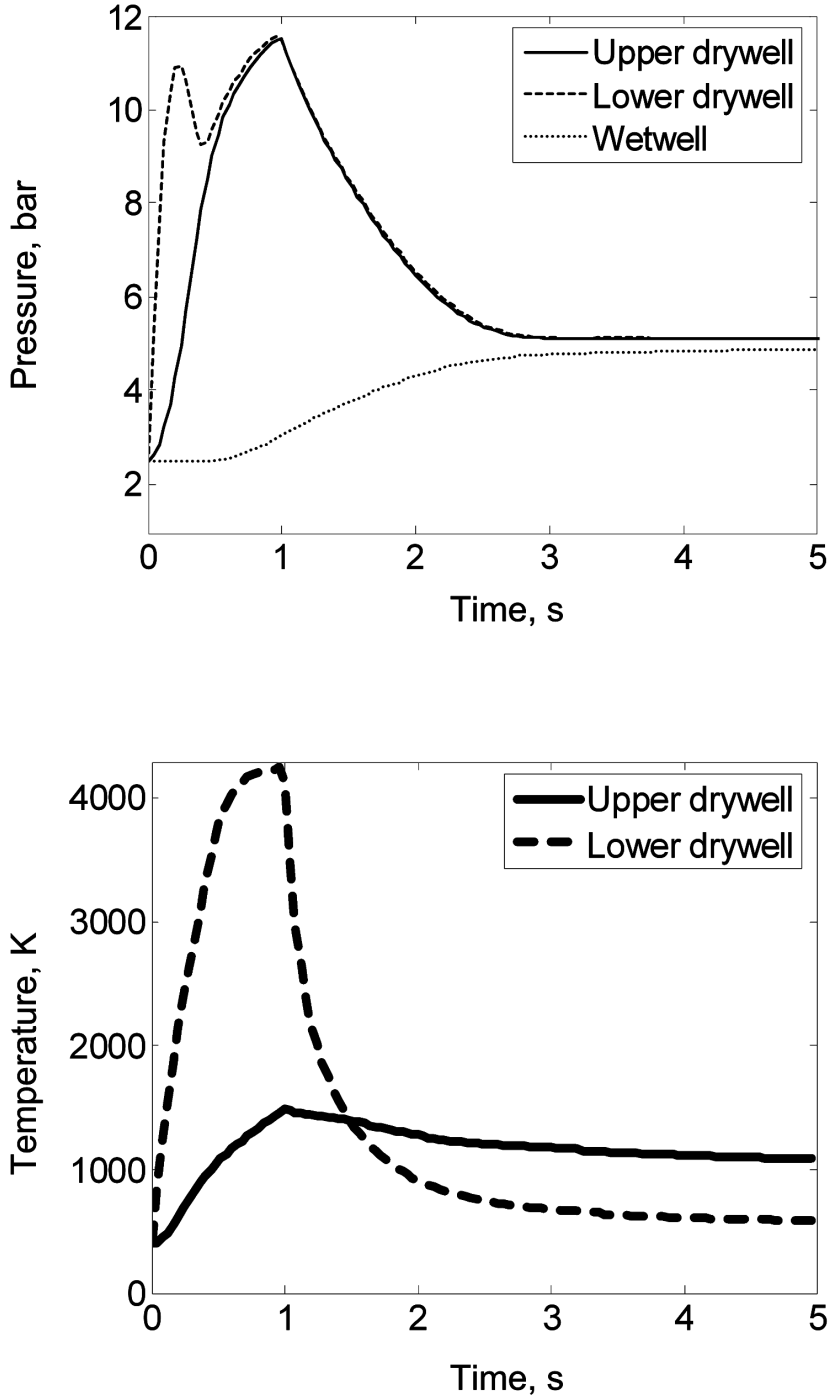

Figure 21.3.4.2-2. Drywell Pressure and Temperature in a Hypothetical Scenario

Drywell pressure (top), and temperature (bottom) in a strictly hypothetical scenario selected to illustrate the effect of vent clearing, and subsequent gas venting, at conditions that approach containment-integrity-challenging levels.

So what remains is to consider the effects of elevated temperatures of the DW atmosphere on liner (and penetration seals) integrity. Clearly this is only relevant to the sequences for which DW sprays are not available, and as noted already (see Figure 21.2-1) these amount to 0.78% of the 1.3% [18%], or ~1% of the CDF. The evaluation is done in the next section, and again we aim for a conservative treatment. Interestingly, in the DCH evaluations for PWRs peak temperatures reached only ~600 K, (620 °F) and they were never an issue—here in a much smaller DW volume, even though it is open, the DCH temperatures can reach considerably higher levels, even in the absence of combustion.

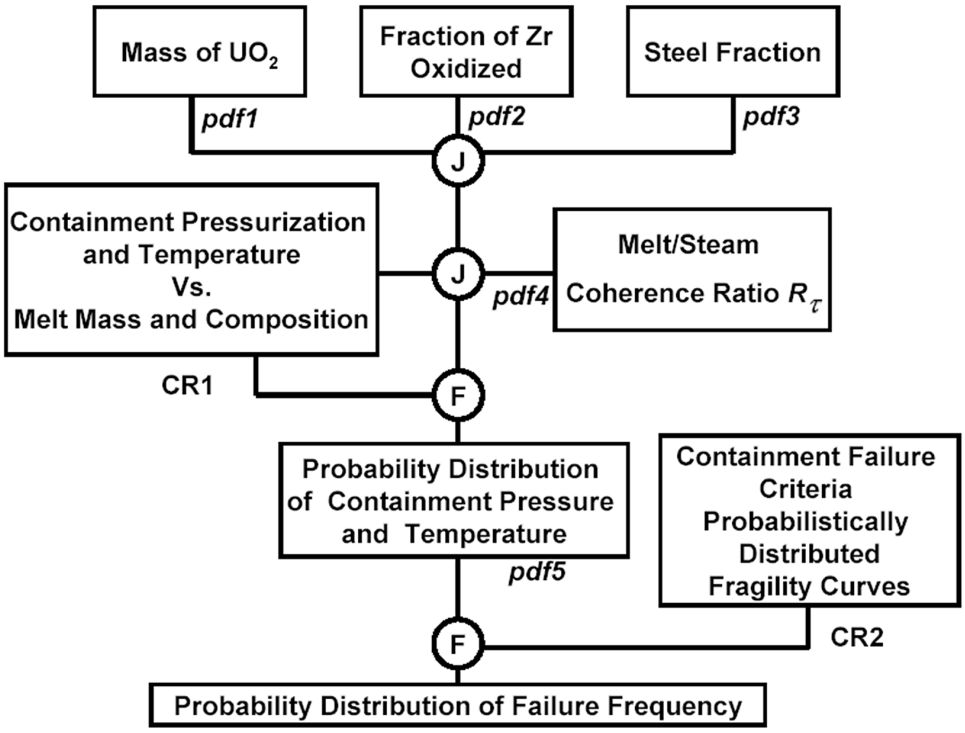

Figure 21.3.4.2-3. Probabilistic Framework of Pwr Dch Issue Resolution
(Theofanous, 1996; Pilch, Yan, Theofanous, 1996).

21.3.4.3 Quantification of DCH Loads

As noted already, we use the CLCH model (Yan and Theofanous, 1993) adapted for present purposes by a rendering that captures the full transient, in an open system, and it's coupling to vent-clearing. The equations, simple mass and energy balances, over the communicating LDW, UDW, and WW volumes, are summarized in Table 21.3.4.3-1. This model was verified by comparison to final pressures/temperatures calculated for the original closed system configuration of the original model, as well as sample IET test results that included the complete transients (see Figure 21.3.4.3-1, and Appendix A).

The vent-clearing model reflects a simple accounting of water inertia, including the added mass effect, in the suppression pool, as it is being accelerated, under the action of the UDW pressure, into the WW. The equations are summarized in Table 21.3.4.3-2. Corium

properties, metal-steam reactions and related energies are treated in the same way as in the previous work leading to resolution of DCH issue for PWRs (Pilch, Yan and Theofanous, 1996). As seen in Figure 21.3.4.3-2 and Table 21.3.4.3-3 (see also Appendix B), the model captures quantitatively the behavior as found in the full-scale, Pressure Suppression Test Facility (PSTF) experiments conducted in support of the LOCA-Loads program by GE (1974).

Finally, in the WW model, the heat losses from the gas stream passing through the suppression pool, which in a DCH event would be highly agitated and grossly dispersed, are accounted through parameters used to reflect the condensation and heat transfer (non-condensable) efficiencies.

Ablation of the initial penetration opening, and of the sacrificial refractory layer on top of the BiMAC during HPME was estimated according to well established models and procedures. The former case involves parallel flow and for it we use the model of Pilch (1994) as done by Pilch, Yan, and Theofanous (1996). The latter case involves impinging flow and for this we use the model of Saito (1991) as done by Theofanous et al (1996). The results for hole ablation are very similar to those obtained previously, yielding final diameters of 0.2 m (8 in) and 0.3 m (12 in) for 100 and 300 metric tons (110 and 330 tons) of melt involved in the expulsion process respectively. In terms of area, this is rather weakly dependent on the number of assumed simultaneous penetration failures, as this is compensated by the shorter duration of the HPME. The evaluation of refractory ablation is presented in Subsection 21.5 (on BMP).

In estimating DCH, in PWRs the principal ingredient in the original model was the DCH-scale (Yan and Theofanous, 1996), and this is used as such in the present application as well. In previous assessments, this quantity was quantified as an intangible parameter, with a most probable value given by Eq.21.3.4.3.1, and a probability distribution around this value assumed to be normal with a standard variation of 12.5% (roughly, and conservatively, based on the quality of agreement with the IET data).

$$R_\tau = \tau_m / \tau_s = 0.2 V_{cav}^{1/3} T_{RCS,0}{}^{1/2} / P_{RCS,0} / \tau_s \qquad (21.3.4.3.1)$$

$P_{RCS,0}$ is the primary system pressure prior to HPME (in MPa), τ_s is the characteristic blowdown time (given in Table 21.3.4.3-1), and tm is the melt entrainment time.

Table 21.3.4.3-1

The Transient CLCH Model

Vessel:

$$\frac{P_{RCS}}{P_{RCS,0}} = \left\{1 + \frac{\gamma - 1}{2}\Gamma\frac{t}{\tau_s}\right\}^{2\gamma/(\gamma-1)}$$

$$\dot{m}_{blowdown} = \eta A_b \rho_{s,0} a_{s0} \Gamma \left\{1 + \frac{\gamma - 1}{2}\Gamma\frac{t}{\tau_s}\right\}^{(\gamma+1)/(1-\gamma)}$$

$$\frac{T_{RCS}}{T_{RCS,0}} = \left(\frac{P_{RCS}}{P_{RCS,0}}\right)^{(\gamma-1)/\gamma}$$

where $a_{s0} = (\gamma R T_{RCS,0})^{1/2}$, $\Gamma = \left[\frac{2}{\gamma+1}\right]^{(\gamma+1)/2(\gamma-1)}$ and $\tau_s = \frac{V_{RCS}}{\eta A_b a_{s0}}$

Lower Drywell:

$$\dot{m}_m = \begin{cases} \frac{m_{m,0}}{\tau_m} & t \le \tau_m \\ 0 & t > \tau_m \end{cases}$$

$$T_{mix} = \frac{\dot{m}_{blowdown} C_{p,s} T_{RCS} + \dot{m}_m C_{p,m} T_m + \dot{m}_{ox} Q_{ox}}{\dot{m}_{blowdown} C_{p,s} + \dot{m}_m C_{p,m}}$$

$$\dot{m}_{ox} = M_m \min\left(\frac{\dot{m}_m}{M_m}, \frac{\dot{m}_{blowdown}}{\nu M_v}\right)$$

$$\dot{m}_{conv} = f(p_{LDW}, p_{UDW}, T_{LDW}, T_{UDW}, A_{connect})$$

$$T_{conv} = \begin{cases} T_{LDW} & \text{if } \dot{m}_{conv} > 0 \\ T_{UDW} & \text{if } \dot{m}_{conv} < 0 \end{cases}$$

$$\frac{d(m_{LDW} C_{v,LDW} T_{LDW})}{dt} = \dot{m}_{blowdown} C_{p,s} T_{mix} - \dot{m}_{conv} C_{p,s} T_{conv}$$

$$\frac{dm_{LDW}}{dt} = \dot{m}_{blowdown} - \dot{m}_{conv}$$

Upper Drywell:

$$\frac{d(m_{UDW} C_{v,UDW} T_{UDW})}{dt} = \dot{m}_{conv} T_{conv} - \dot{m}_{vent} T_{UDW}$$

$$\frac{dm_{UDW}}{dt} = \dot{m}_{conv} - \dot{m}_{vent}$$

Wetwell:

$$\dot{m}_{H_2,WW} = f_{H_2}^{UDW} \dot{m}_{WW}$$

$$\dot{m}_{N_2,WW} = f_{N_2}^{UDW} \dot{m}_{WW}$$

$$\dot{m}_{H_2O,WW} = (1 - f_{H_2O}^{condense}) f_{H_2O}^{UDW} \dot{m}_{WW}$$

$$\frac{dm_{WW}}{dt} = \dot{m}_{H_2,WW} + \dot{m}_{N_2,WW} + \dot{m}_{H_2O,WW}$$

$$\frac{d(m_{WW} C_{v,WW} T_{WW})}{dt} = \left(\dot{m}_{H_2,WW} C_{p,H_2} + \dot{m}_{N_2,WW} C_{p,N_2} + \dot{m}_{H_2O,WW} C_{p,H_2O} \right) T_{WW}^{condense}$$

$$T_{WW}^{condense} = T_{UDW} (1 - \psi_{WW}) + T_{WW} \psi_{WW}$$

$$P_{WW} = \frac{m_{WW}}{M_{WW}} \frac{RT_{WW}}{V_{WW}}$$

Table 21.3.4.3-2. The Vent Model

Vertical Vent:

$$\left\{ \frac{A_v}{nA_h}(L+D_h)+(H-z)\right\}\rho\frac{du}{dt}=P-\left(P_0+\rho gz\right)-\frac{1}{2n^2}\left(\frac{A_v}{A_h}\right)^2\rho u^2(1+C_{d,junc});\quad u=\frac{dz}{dt}$$

(n is the number of vents yet to be cleared).

Horizontal Vents:

For $z > Z_i$: $(L+D_h)\rho\frac{du_h}{dt}=P-\left(P_0+\rho gz\right)-\frac{1}{2}\rho u_h^2;\qquad u_h=\frac{dx}{dt}$

Venting Rate:

$$\dot{m}_{vent}=\sum_i \delta_i f(p_{UDW}, p_{SP}+\rho_W g Z_{i,h}, T_{UDW}, T_{SP}, A_i)$$

$$\delta_i=\begin{cases}0 & \text{if } x_i \le L\\ 1 & \text{if } x_i > L\end{cases}$$

$$\dot{m}_{SP}=\dot{m}_{vent}\eta_{nc,UDW}$$

For details of the vent model derivation and nomenclature, see Appendix B.

Table 21.3.4.3-3

Summary of Predictions against Experimental Data

Test Series	Description	Data	TRACG	Present
5703-01	a. Short-term peak pressure, kPa (psia)	193 (28.0)	200 (29.0)	205 (29.7)
	b. Vent clearing time (s)		0.85	
	- Top vent	0.86	1.15	1.18
	- Middle vent	1.15	DNC	1.48
	- Bottom vent	DNC		DNC
5703-02	a. Short-term peak pressure, kPa (psia)	200 (29.0)	227.5 (33.0)	230 (33.4)
	b. Vent clearing time (s)			
	- Top vent	1.14	1.05	1.42
	- Middle vent	1.52	1.35	1.68
	- Bottom vent	DNC	DNC	DNC
5703-03	a. Short-term peak pressure, kPa (psia)	252 (36.5)	289.6 (42.0)	293 (42.5)
	b. Vent clearing time (s)			
	- Top vent	0.99	0.85	1.16
	- Middle vent	1.19	1.05	1.35
	- Bottom vent	1.60	1.30	1.93
Note:	DNC denotes vent “do not clear”.			

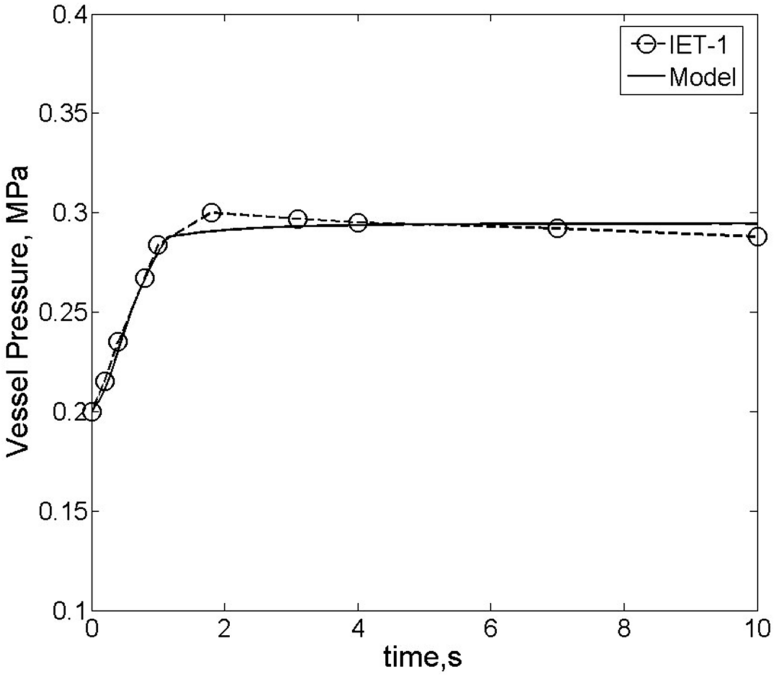

Figure 21.3.4.3-1. Prediction of DCH Pressure in SNL IET-1 Test

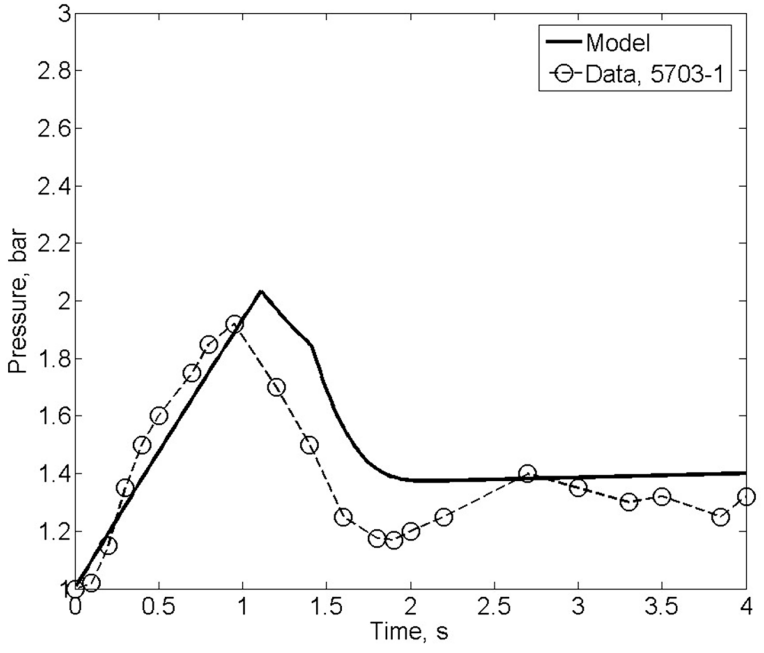

Figure 21.3.4.3-2. Prediction of Drywell Pressure in PSTF Test 5703-1

Table 21.3.4.3-4. Geometry and Initial Conditions in Reactor Calculations.

Compartment	Parameter	Definition	Value
Primary System	V_{RCS}, m^3 (ft^3)	Volume of RCS	500 (18,000)
	P^0_{RCS}, MPa (psia)	Pressure of RCS at blowdown	8 (1200)
	T^0_{RCS}, K (°F)	Temperature of RCS at blowdown	800 (980), 1500 (2200)
	D_S, m (in)	Vessel breach size (diameter)	0.2 (8), 0.3 (12), 0.5 (20)
Upper Drywell	V_{UDW}, m^3 (ft^3)	Volume of upper drywell	6016 (212,500)
	P^0_{UDW}, MPa (psia)	Initial pressure of upper compartment	0.25 (36)
	T^0_{UDW}, K (°F)	Initial temperature of upper	300 (80)
	$A_{connect}$, m^2 (ft^2)	Area connecting upper and lower	14 (150)
Lower Drywell	V_{LDW}, m^3 (ft^3)	Volume of lower compartment	1190 (42,000)
	P^0_{LDW}, MPa (psia)	Initial pressure of lower compartment	0.25 (36)
	T^0_{LDW}, K (°F)	Initial temperature of lower compartment	300 (80)
Wetwell	A_{pool}, m^2 (ft^2)	Total area connecting the upper	16 (170)
	D_{vent}, m (in)	Diameter of horizontal vent	0.7 (28)
		Number of rows of horizontal vents	3
	m, (in)	Distance between top and middle vents	1.37 (53.9)
	m, (in)	Distance between middle and bottom vents	1.37 (53.9)
	H, m (ft)	Height of water for clearing vent	Max. 5.45 (17.9)
	$V_{WW,}$ m^3 (ft^3)	Wetwell (free) volume	5400 (191,000)
Corium	m^0_m, metric tons (tons)	Initial corium mass in the lower drywell	50 (55), 100 (110), 300 (330)
	f_{Zr}	Mass fraction of metal Zr in corium	20%
	T^0_m, K (°F)	Initial corium temperature	2800 (4600)
	$\Delta T^0_{m,sol}$, K (°F)	Initial superheat of molten corium	300 (540)

Table 21.3.4.3-5.

Summary of Parameters and Variables in Reactor Calculations

Parameter	Parameter Definition	Reactor Case							
		A	B	C	D	E	F	G	H
m_m^0, metric tons (tons)	Initial mass of corium in the lower drywell	50 (55)	50 (55)	100 (110)	100 (110)	300 (330)	300 (330)	300 (330)	300 (330)
D_S, m (in)	RPV hole size for steam blowdown	0.2 (8)	0.2 (8)	0.2 (8)	0.2 (8)	0.3 (12)	0.3 (12)	0.5 (20)	0.5 (20)
T_{RCS}^0 K (°F)	Initial temperature in the primary system	800 (980)	800 (980)	800 (980)	1500 (2200)	800 (980)	800 (980)	800 (980)	800 (980)
τ_m (s)	Mixing time between melt and blowdown steam	7.8	3.6	10	10	7.8	10	3	6

Note: A set of common parameters used in reactor calculations (A-H cases) includes:

Φ - Fraction of metal in entrained melt participating in steam-metal oxidation during blowdown; $\Phi = 0.5$

α - Fraction of blowdown steam interacting with melt; $\alpha = 1$.

$f_{H_2O}^{condense}$ - Efficiency of steam condensation in the suppression pool; $f_{H_2O}^{condense} = 1$.

ψ_{WW} - - Effectiveness of gas-coolant heat transfer in the suppression pool; $\psi_{WW} = 0.5$.

Table 21.3.4.3-6.

Summary of Results from Reactor Calculations

Parameter	Parameter Definition	Reactor Case							
		A	B	C	D	E	F	G	H
τ_s (s)	Blowdown time scale	28.7	28.7	28.7	28.7	12.8	12.8	4.6	4.6
R= τ_m / τ_s	DCH scale	0.27	0.14	0.35	0.35	0.61	0.78	0.65	1.3
P_1, bar (psia))	First (before vent clearing) pressure peak	3.35 (48.6)	3.3 (48)	3.3 (48)	3.1 (45)	4.0 (58)	4.0 (58)	4.7 (68)	4.7 (68)
P_2 ,bar (psia)	Second pressure peak	3.2 (46)	3.1 (45)	3.5 (51)	3.0 (44)	4.2 (61)	4.8 (70)	6.0 (87)	6.0 (87)
P_∞ bar (psia)	Long-term pressure	3.3 (48)	2.8 (41)	3.5 (51)	3.2 (46)	4.5 (65)	5.1 (74)	4.3 (62)	6.5 (94)
T_{STAB} ,K (°F)	Stabilized temperature	600 (620)	500 (440)	750 (890)	800 (980)	900 (1200)	1000 (1300)	1000 (1300)	1200 (1700)

Applied here as an example, at ESBWR conditions (800 K (980 °F), 8 MPa (1200 psia), and 1,320 m^3 (46,600 ft^3) LDW volume), Equation 1 yields τ_m = 7.8 s. Thus, for 1 m (3 ft) break considered in the previous section, the blowdown time constant is τ_s =1.1 s, and the appropriate (for reference) DCH-scale value would then be ~7. This means the blowdown would provide for full participation of steam in the DCH process (no incoherence). On the other hand, for a more reasonable break size, say the one noted as bounding the creep rupture type of vessel breach (0.5 m, 20 in), the blowdown time constant would be 4.4 s, and the same melt entrainment time would produce a DCH scale of ~2, that is still in the full utilization regime. Mitigation due to incoherence occurs only for penetration-type failures (0.2 to 0.3 m (8 to 12 in) breaks), which yield quite long blowdown times and DCH scale values of 0.3 and 0.65 respectively. Thus, immediately we can see that larger breaks involve not only stronger dynamics but also greater utilization of the steam in producing DCH loads.

These trends can be seen in a more tangible manner in the results of a series of calculations run for this purpose, as well as for the purpose of demonstrating upper bounds on pressurization and the margins to failure still available. The reactor data used in these calculations are summarized in Table 21.3.4.3-4, and the model parameter choices made to scope out the range of behavior are given in Table 21.3.4.3-5. As noted already the intent in choice of break areas is to span the range from an upper bound creep-type breach (cases G and H) to the more realistic penetration-type failures. Further we explore the sensitivity to the quantity of the melt involved, all the way to the maximum amount possible (300 metric tons, 330 tons), and also to the melt ejection time with parametric choices selected around the predicted value of 7.8 s. The sensitivity to the initial melt temperature is negligible, and in any case we use a conservatively low value of 800 K (980°F) (the loads decrease with increasing steam temperature). All key results are summarized in Table 21.3.4.3-6, which will be used in the discussion that follows, along with Figures 21.3.4.3-3 to 21.3.4.3-10 depicting the calculated pressure transients, and Figure 21.3.4.3-11 depicting the temperatures obtained for the various cases.

Starting from the two large breech area cases (G and H), we see the same basic features as in the arbitrary-bounding case considered in the previous section, except that they are less accentuated. Now, rather than a peak in pressure of the LDW we have an inflection point, but the LDW and UDW pressures again equalize, and again there is a rapid cool-down following the melt entrainment period. However, there is also an essential difference in the dynamics of these two cases. The one with the rapid dispersal (case G) exhibits a peak pressure in the early, highly dynamic domain that does not involve, yet, the WW. The other (case H), with a more appropriate dispersal time, exhibits a double peak, the first being very similar to that of case G, while the second being of a quasi-static nature, and involving fully the WW volume. The two peaks are, quite coincidentally, of similar magnitudes (0.6 vs. 0.66 MPa, 87 vs 96 psia). Now with reference to Table 21.3.4.3-6, we see that the DCH scales for these two cases are 0.65 and 1.3. This means that case G is steam-limited (note a final pressure of only 0.43 MPa, 62 psia), while case H is already close to the asymptotic regime of Yan and Theofanous (1996) — any further increases of the melt entrainment time would not lead to increased pressure levels beyond the 0.65 MPa (94 psia) found here. This quasi-static regime is also seen to dominate cases E and F. Here the DCH scale is less than 1, indicating the process is steam-starved. Indeed, the somewhat greater final pressure in F is due to differences in the amount of this steam limitation

(DCH scale values of ~0.6 and ~0.8). This quasi-static behavior, and effects of melt-steam incoherence, become more dramatic, as the breech area is further reduced, and the DCH scale, as a consequence gets even smaller (0.14 to 0.35) – cases A to D. These effects are also apparent in the UDW temperatures, reducing from a maximum value of ~1,200K (1700°F) for the near asymptotic case (H), down to 500K (440°F), as the DCH scale reduces from 1.3 down to 0.14.

As we will see in the next section these temperature levels would be of no concern to liner integrity, however, we do note that the LDW is subject, albeit for very short periods of time, to levels that can reach 4,000 K (6700°F). In addition, in a postulated HPME and dispersal event, one would expect that melt, perhaps in significant quantities would contact the LDW liner. Both processes can induce local failures, and there is no way to know how likely this would be, except that (a) the situation could be possibly avoided if there is natural depressurization (the splinter discussed in Section 3.4.2), and (b) the melt might be effectively captured by the BiMAC device. Since both remedies are speculative, the potential for failure is acknowledged in the CPETs (see Section 6) and the Level-3 PRA.

See also Addendum to this Section at the end of Section 21.3.

Case A

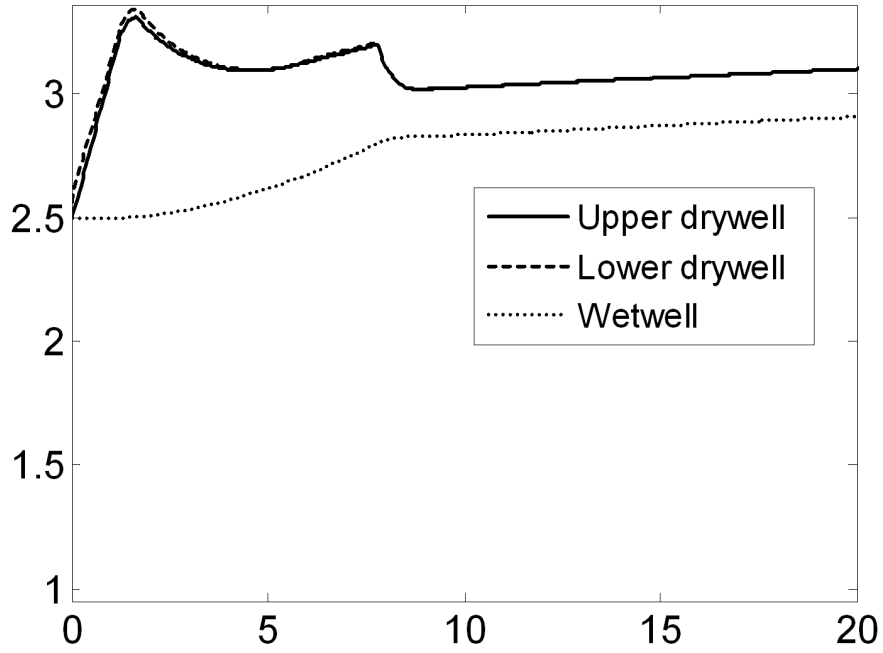

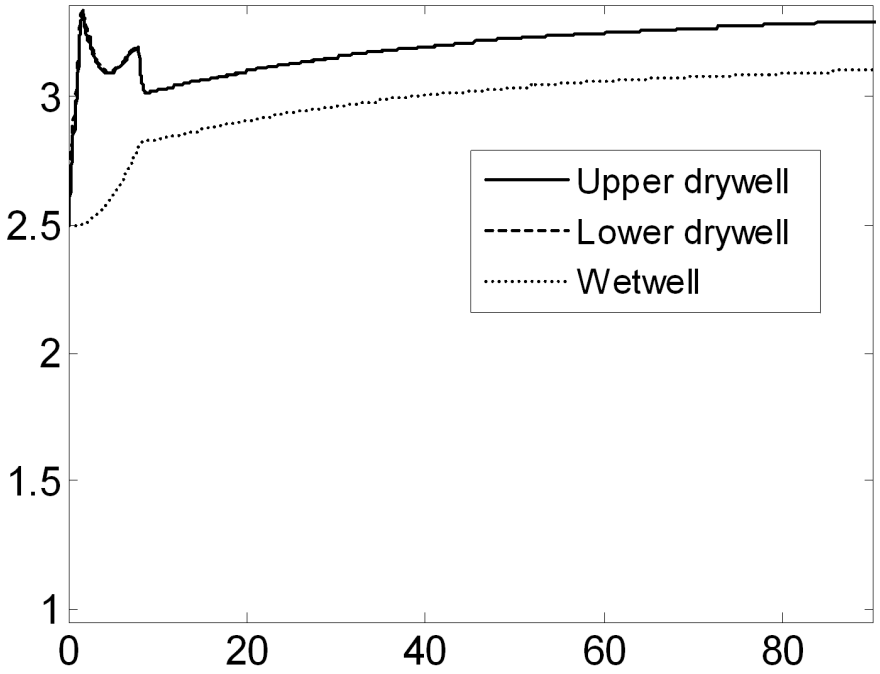

Figure 21.3.4.3-3. Predictions of Pressures of in the DW and WW for Case A

Predictions of pressures of in the DW and WW for Case A (pressures in the UDW and LDW follow each other closely, and are hardly distinguishable).

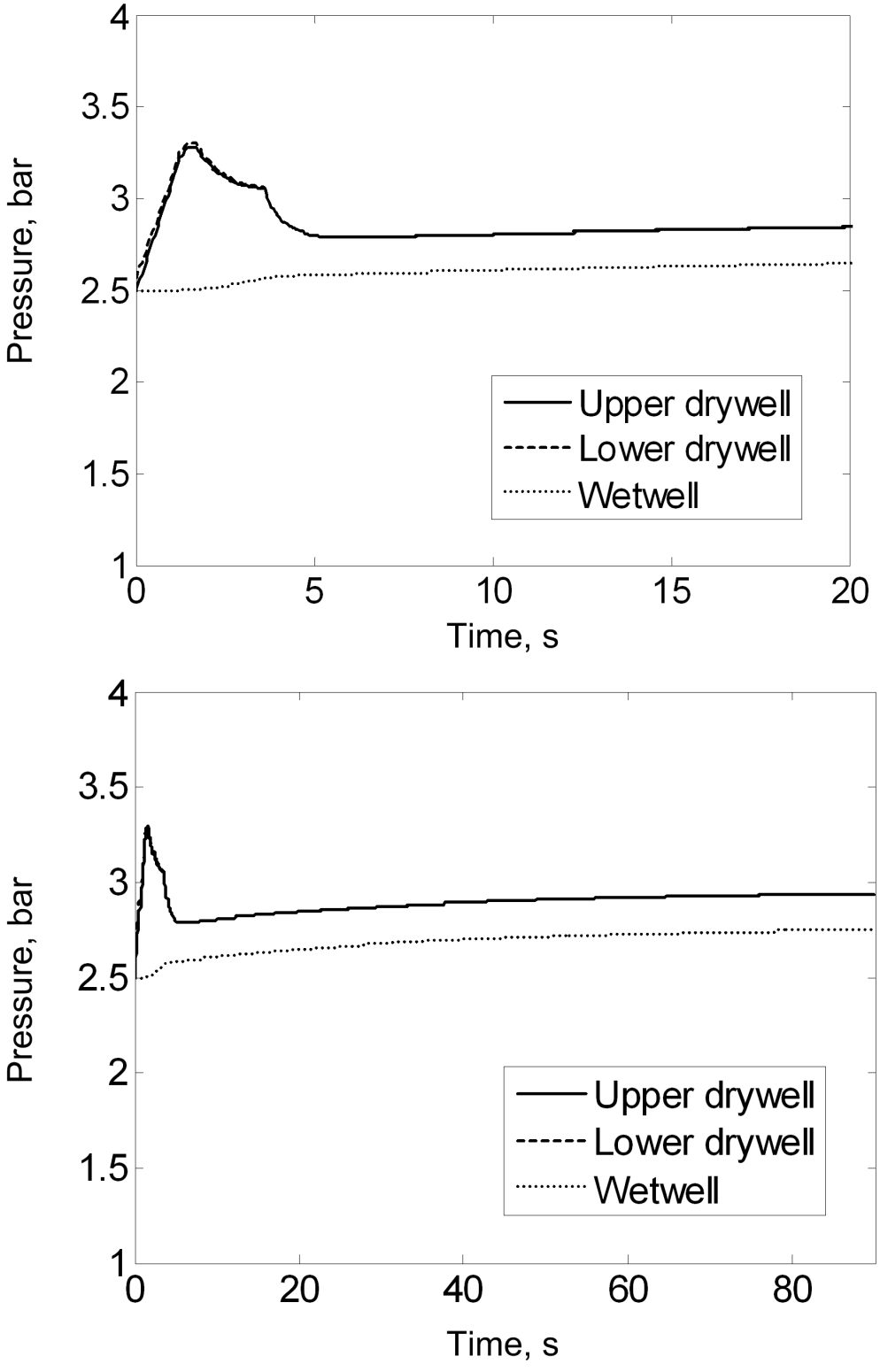

Figure 21.3.4.3-4. Predictions of Pressures of in the DW and WW for Case B

Case C.

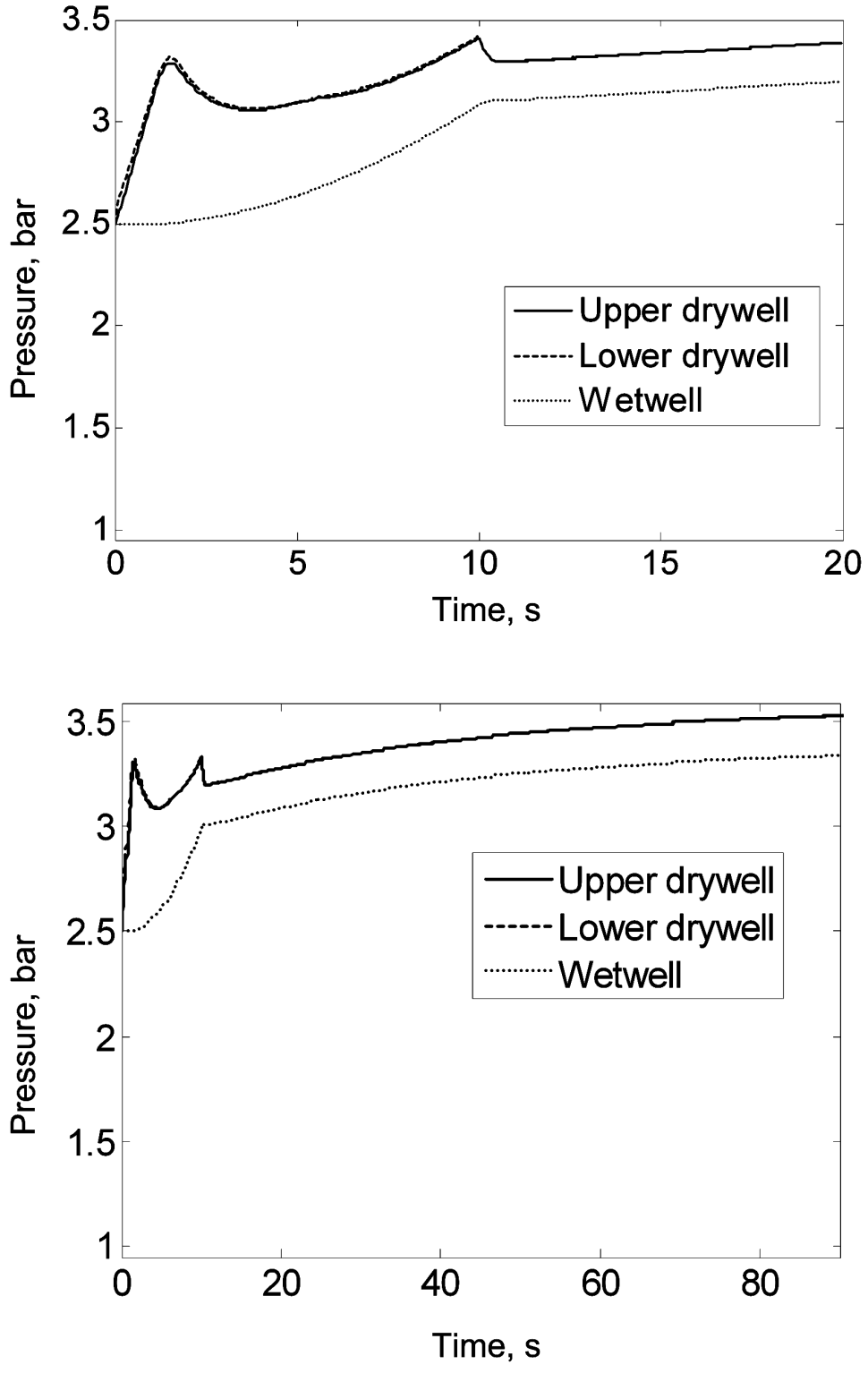

Figure 21.3.4.3-5. Predictions of Pressures of in the DW and WW for Case C

Case D.

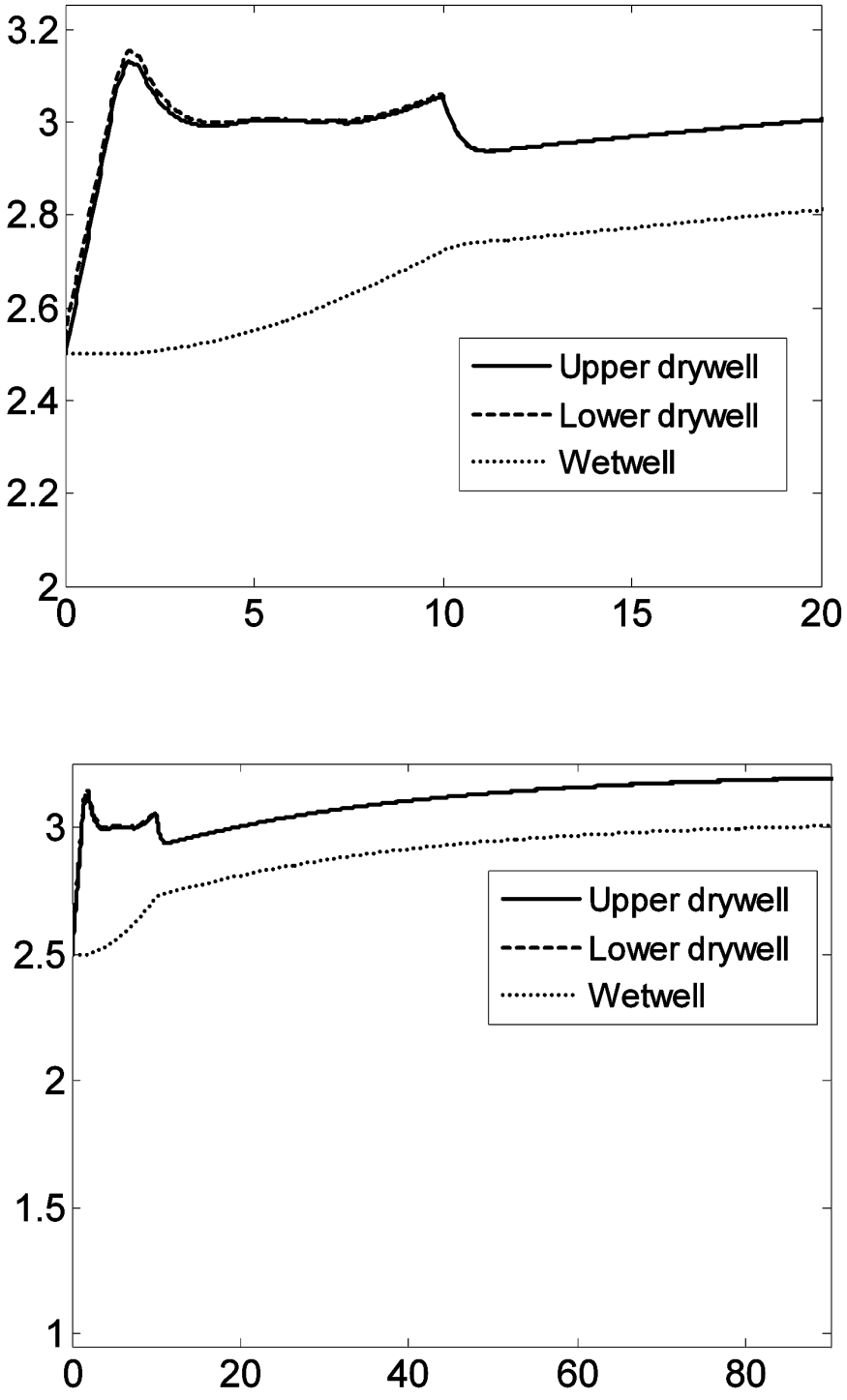

Figure 21.3.4.3-6. Predictions of Pressures of in the DW and WW for Case D

Case E

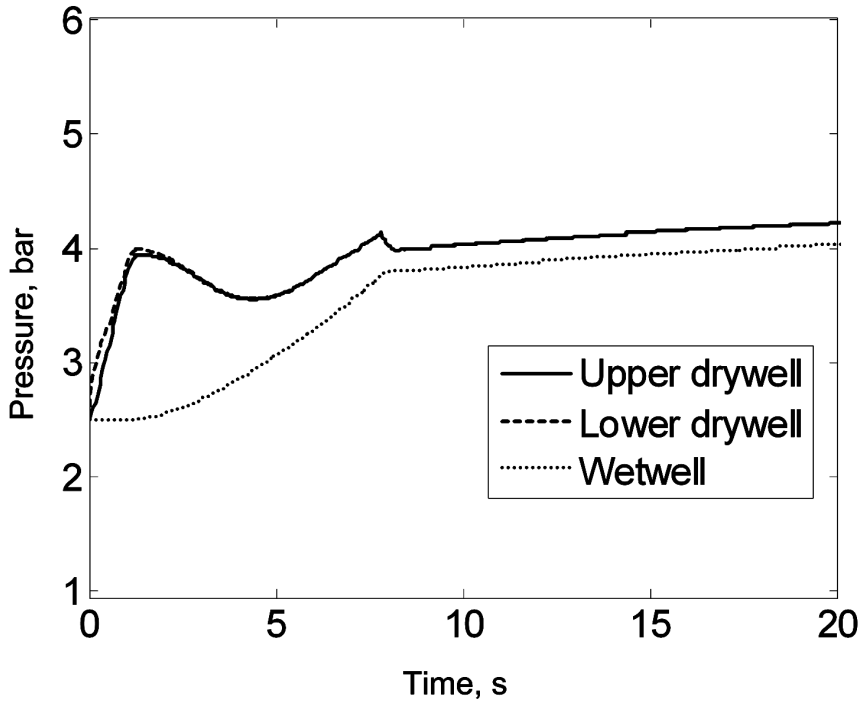

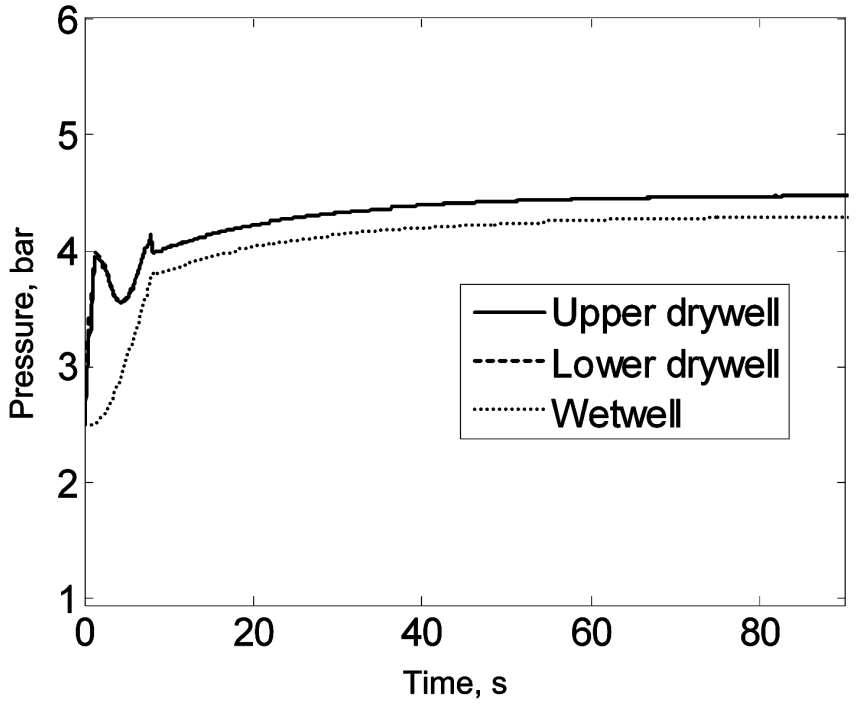

Figure 21.3.4.3-7. Predictions of Pressures of in the DW and WW for Case E

Case F

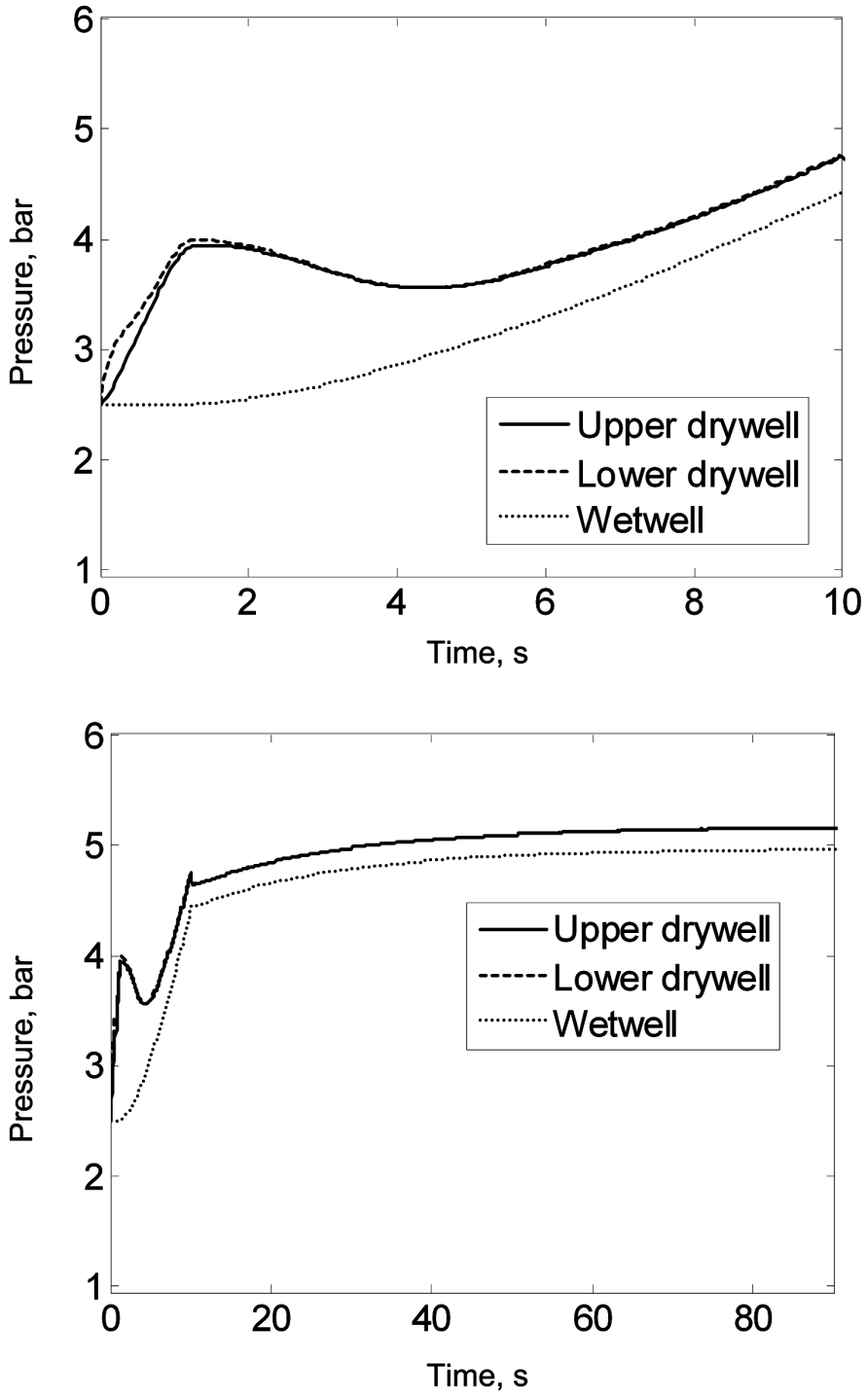

Figure 21.3.4.3-8. Predictions of Pressures of in the DW and WW for Case F

Case G

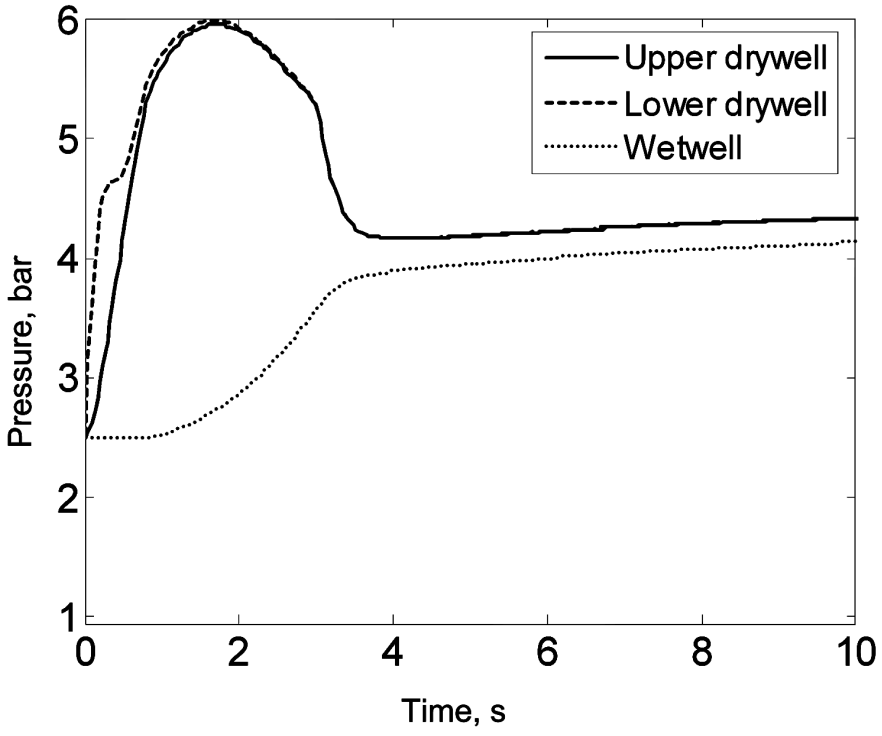

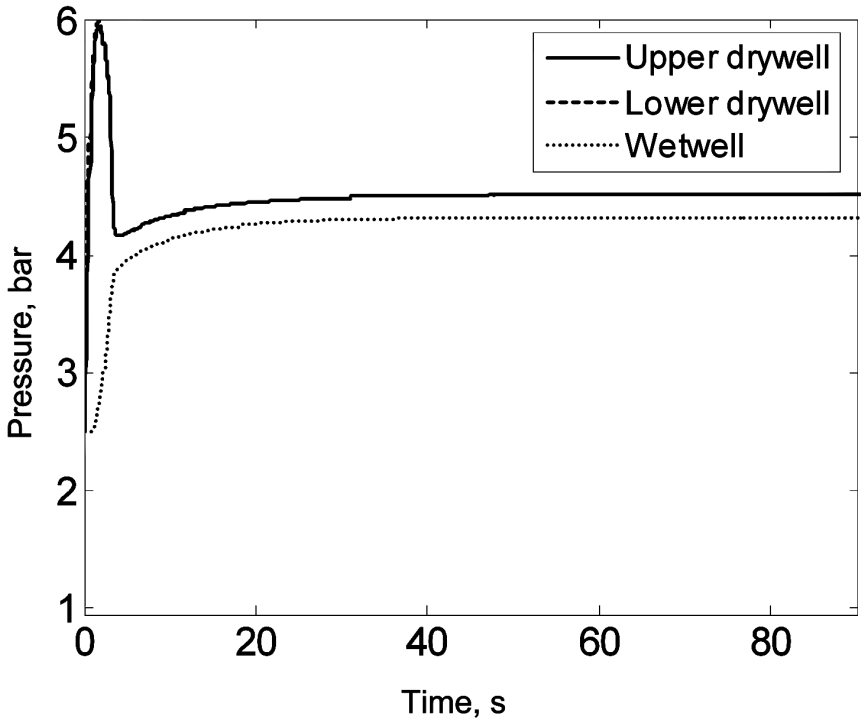

Figure 21.3.4.3-9 Predictions of Pressures of in the DW and WW for Case G

Case H

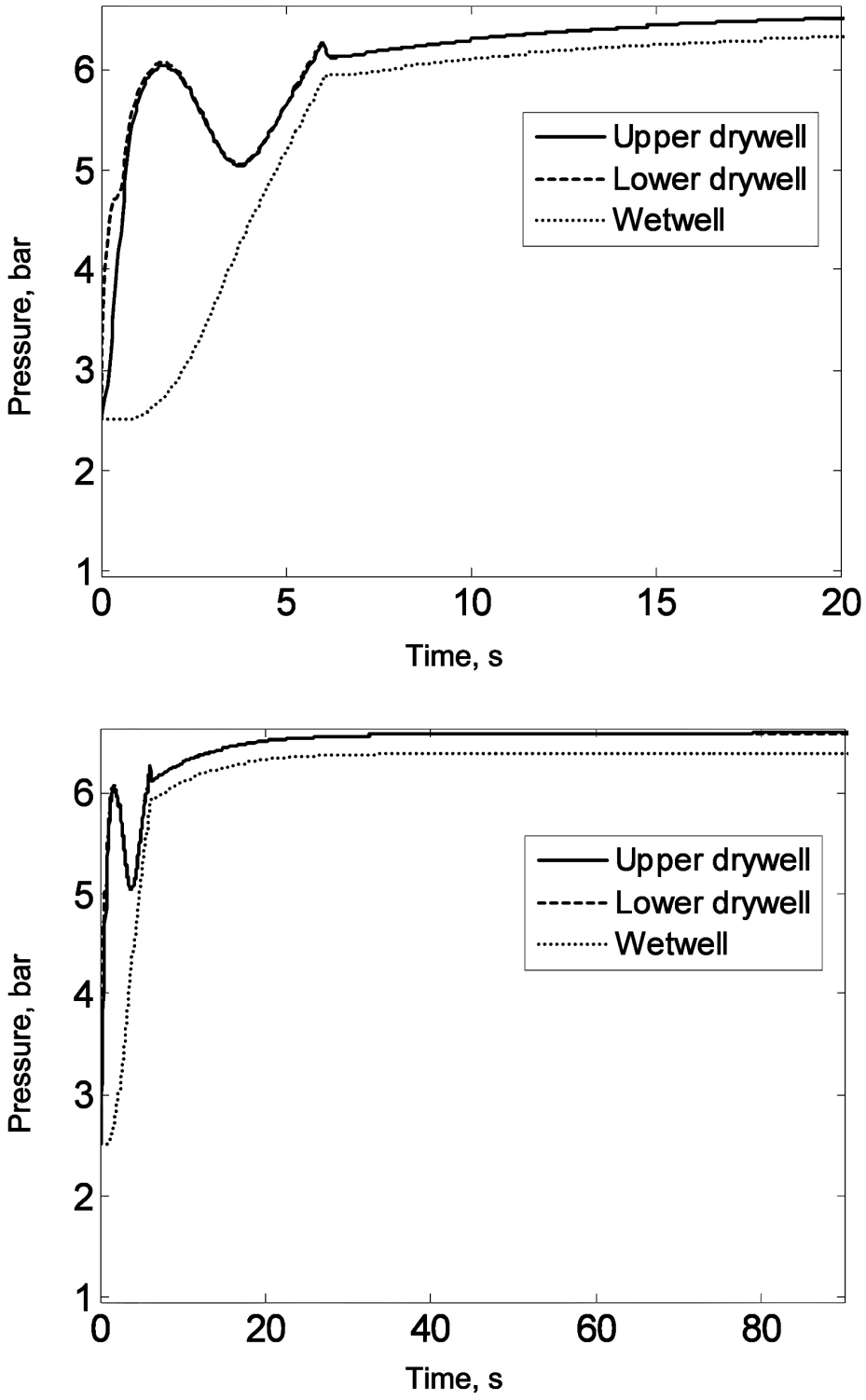

Figure 21.3.4.3-10 Predictions of Pressures of in the DW and WW for Case H

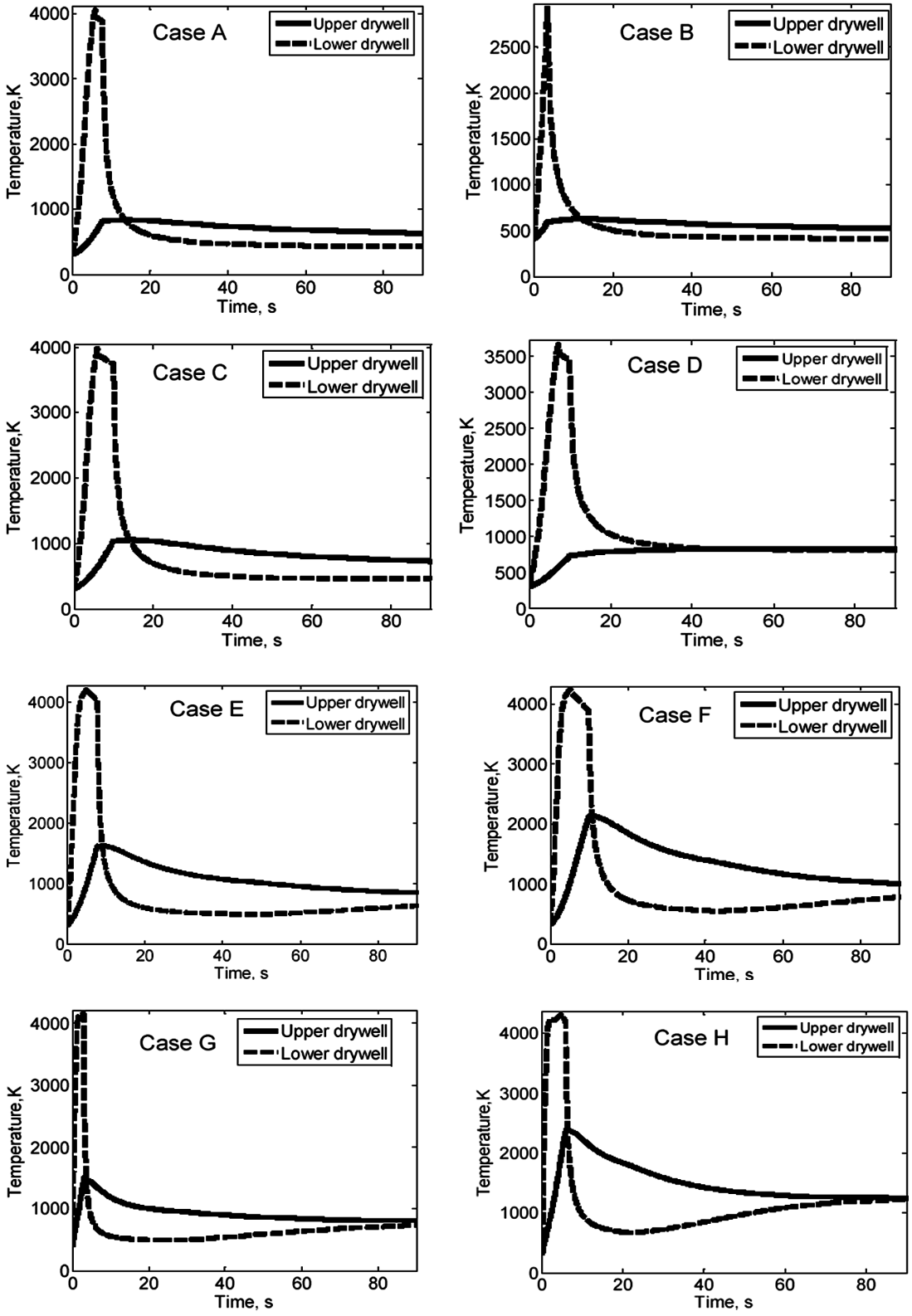

Figure 21.3.4.3-11. Predictions of Gas Temperatures in the LDW and UDW

21.3.4.4 Quantification of Fragility to DCH

The ultimate capacity of the ESBWR containment structures, as documented in Section 8 of NEDO-33201 Revision 1, is summarized in Table 21.3.4.4-1. For DCH pressure loads, only the low temperature entries in this table are relevant. As we can see, the limiting component is the (torispherical steel) DW Head, estimated to be subject to incipient failure at a pressure level of ~1.2 MPaG (170 psig). The complete fragility, plotted from data supplied in the same document is shown in Figure 21.3.4.4-1. [An updated Probabilistic Analysis for Containment Pressure Fragility is included in DCD Appendix 19C. The pressure capability of the Drywell Head in DCD Appendix 19C Table 19C-13, 1.095 MPaG (158.8 psig) at 533 K (500°F) is consistent with the values in Table 21.3.4.4-1, 1.20 MPaG (174 psig) at 500 K (440°F).]

Table 21.3.4.4-1

Ultimate Pressure Capabilities of the ESBWR Containment

(Evaluated at the 97% confidence level)

Structural Component	Ultimate Pressure Capability MpaG (psig)		
	Ambient	~500 K (440°F)	~800 K (980°F)
Wetwell	4.33 (628)	3.90 (566)	1.94 (281)
Upper Drywell	4.80 (696)	4.32 (627)	1.89 (274)
Lower Drywell (Pedestal)	2.85 (413)	2.57 (373)	1.16 (168)
Suppression Pool Slab	1.47 (213)	NA	NA
Basemat	3.63 (526)	3.26 (473)	
Drywell Head	1.49 (216)	1.20 (174)	1.13 (164)

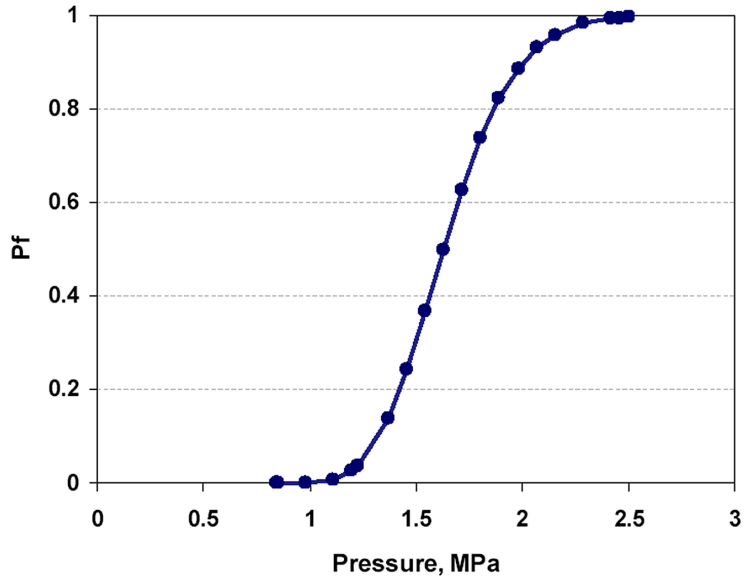

Figure 21.3.4.4-1. The Drywell Head Fragility to Internal Pressure Loads

(Data is obtained from Section 8 of NEDOC-33201 Revision 1).

Consideration of thermal expansion loads inducing liner buckling at the knuckle joint of the torispherical to the cylindrical sections of the TDH, and at the liner anchors, did not lead to concerns about liner failure at temperatures of up to 800 K (980 °F). Further calculations were carried out using DYNA3D (2005) for temperatures reaching up to 1650 K (2510 °F). The temperature-dependent material properties utilized in these calculations are shown in Figure 21.3.4.4-2. A piece of liner in-between a neighboring set of anchors was considered and the presence of concrete backing was taken into account. The results as shown in Figure 21.3.4.4-3 indicate that creep is effective in releasing localized stresses, and that liner integrity is assured for temperatures up to near melting.

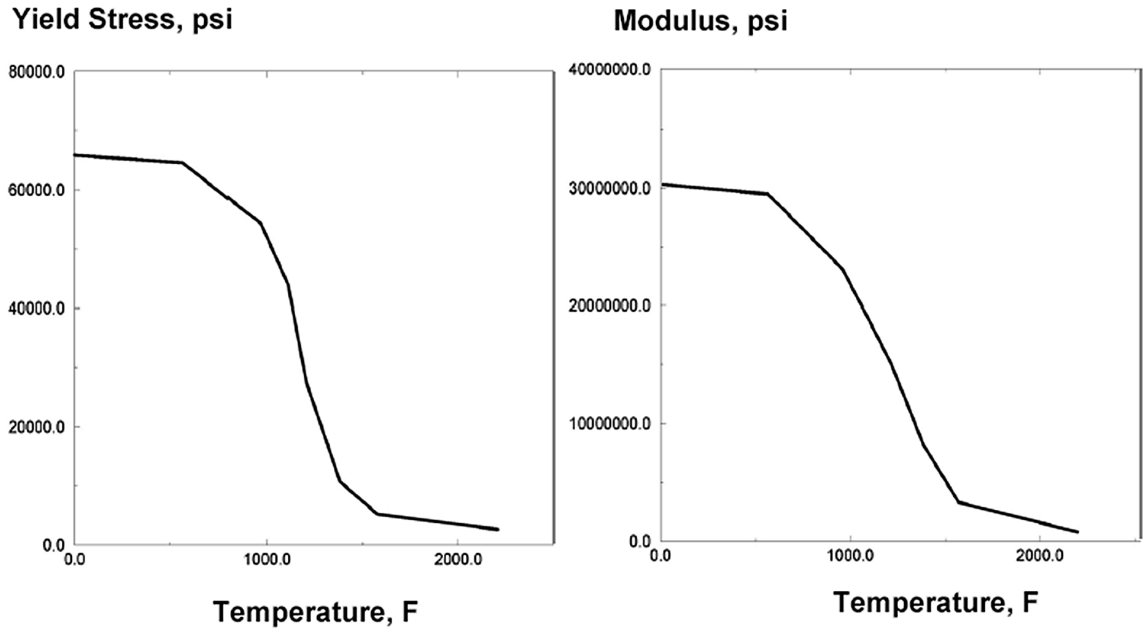

Figure 21.3.4.4-2. Temperature-Dependent Steel Properties

Temperature-dependent steel properties utilized in the finite element calculations of liner subjected to DCH thermal loads, (from Rashid, 1997).

Finally we address the UDW Head, and it's sealing to the cylindrical top portion of the UDW. First we note that during normal operation this head is immersed in a water pool, and thus it remains cold during the whole duration of a HP meltdown sequence, even as the RPV heats up, and is in irradiative heat exchange with it. Bounding estimates of this process yield internal DW Head temperatures of less than 450 K (350 °F), which is well within the range depicted in Table 21.3.4.4-1. This external cooling would be effective also in the long term, and quite sufficient in accommodating the thermal loads from the hot UDW atmosphere as it may develop during a DCH event. In fact, as shown in Figure 21.3.4.4-4, the access of these hot gases to the UDW is so extremely limited that any further heat transfer consideration in this regard would be rather superfluous.

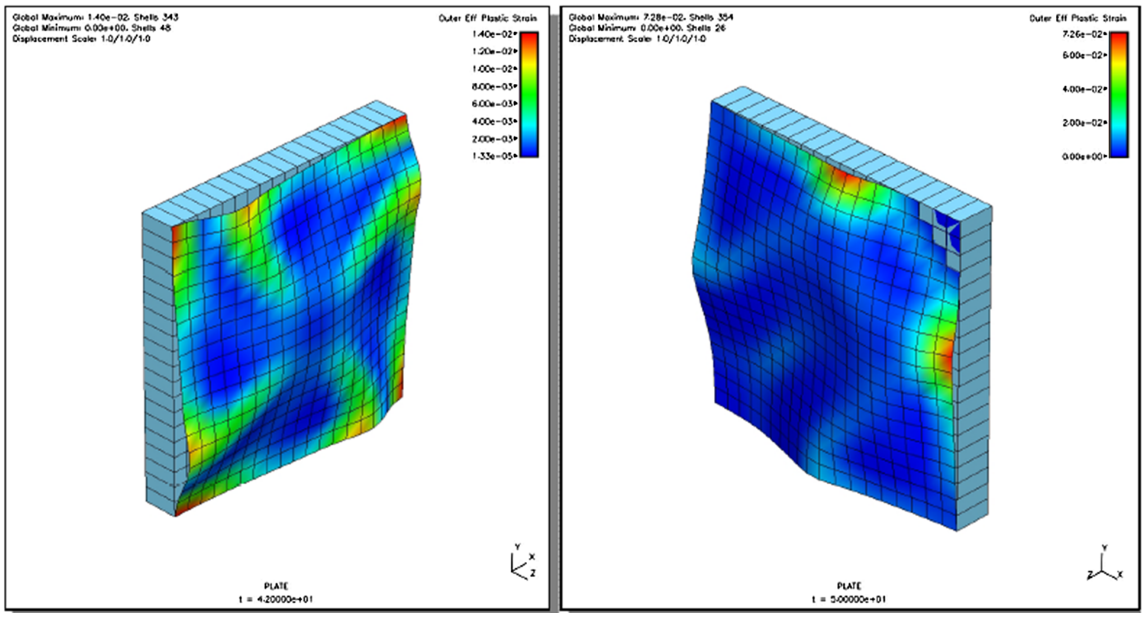

Figure 21.3.4.4-3. Effective Plastic Strains in a Piece of Liner in-Between Anchors

Effective plastic strains in a piece of liner in-between anchors at temperatures of 1400 K (left) and 1650 K (right). Maximum values calculated for the two cases are 1.4% and 7.26% respectively.

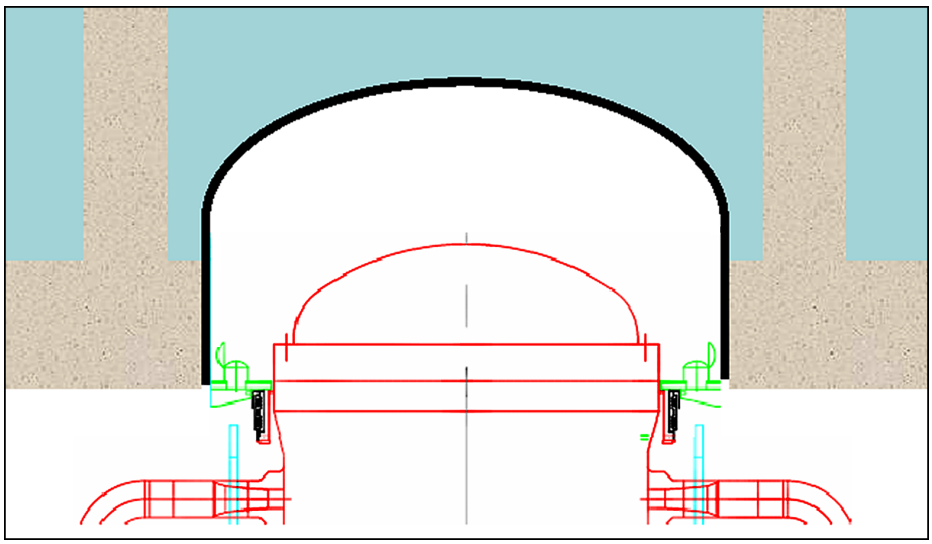

Figure 21.3.4.4-4 Upper drywell between the UDW head and the RPV

The upper drywell compartment (10.4 m diameter) contained between the UDW Head (in black) and the RPV Head (in red) is separated from the UDW's remaining volume by a refueling seal skirt (in green) with 4 access holes (each of 0.4 m^2 area), which are open during normal operation. Also shown is the water pool (blue) on top.

21.3.4.5 Prediction of Failure Probability due to DCH

Taken together the results of the previous two sections show that overpressure (catastrophic) failure of the ESBWR containment due to DCH is physically unreasonable. This conclusion covers all Class III accidents; that is, 1.3% [18%] of the CDF. The margin to failure, as shown by the bounding estimates of loads (upper bound) and fragility (lower bound) in Figure 21.3.4.5-1 are great indeed.

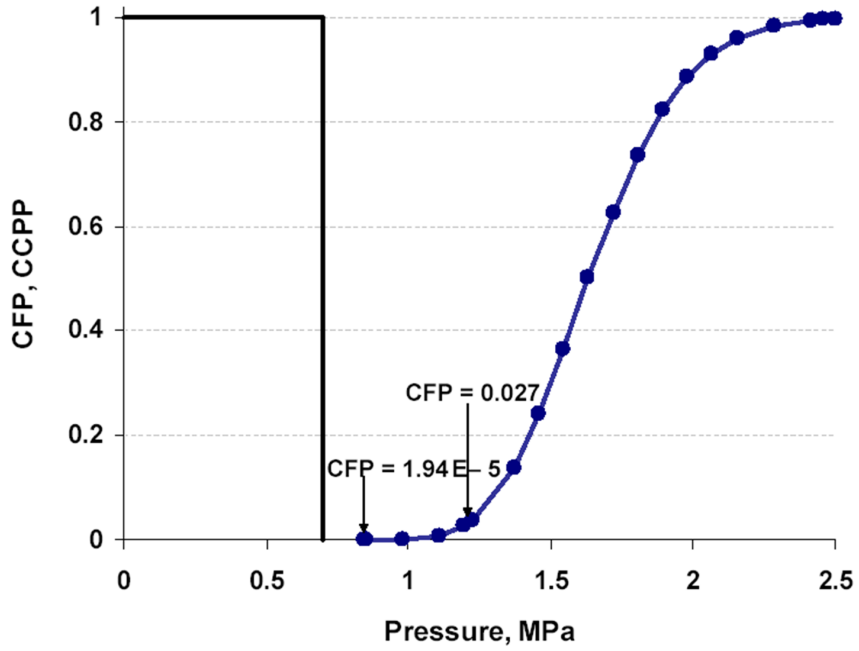

Figure 21.3.4.5-1. Margins to Catastrophic Failure in a DCH Event

The margins to catastrophic failure in a DCH event, bounded at both ends. CFP is the ESBWR containment drywell head's cumulative failure probability. CCPP is the complementary cumulative pressure (load) probability due to DCH. The latter is shown by an upper bound of 0.7 MPa (100 psia), which is case G, adjusted for an initial containment pressure of 0.4 MPa (58 psia), which is the maximum found in analyses of the core-degradation period in the Level II PRA analyses.

Thermally induced failure of the UDW Head and/or its seals is also physically unreasonable for all Class III accidents, as explained in the previous section.

Thermally induced failure of the liner, including the penetration areas, is relevant to Class III accidents in which DW spray is assumed to be not available, and these sequences amount to ~1% [18%] of the CDF. We find that even in these cases, strains due to thermal stresses are rather modest (< 8%) in relation to what might be considered necessary for cracking or tearing, even at temperatures approaching the melting point of the material. Bounding calculations of DCH-induced UDW temperatures indicate that the relevant temperature levels are ~1,000 K (1300 °F), which is considerably below the near-melting temperatures (over 1650 K, 2510 °F) that could cause failure.

However, these calculations also show short periods of potentially very high temperatures in the LDW atmosphere (up to 4000 K, 6700 °F). This, and the presence of potentially large quantities of melt in the LDW, indicate that the LDW liner could be subject to local failures, a condition that is noted in our HP CPET and is accounted for in Level-3 PRA.

21.3.5 Summary and Conclusions for DCH

The above results show that the ESBWR containment can withstand bounding DCH pressure loads and that catastrophic containment failure due to DCH is physically unreasonable.

Principal ingredients to such a conclusion can be recapitulated as follows:

(1) The UDW atmosphere can vent into the WW through a large vent area and an effective heat sink,

(2) The DW head is (externally) immersed in water, and essentially isolated, from the UDW atmosphere,

(3) The containment steel liner is structurally backed by reinforced concrete, which cannot be structurally challenged by DCH.

Moreover, it is important to note that we have identified a splinter scenario for creep failure of the main steam line due to it being heated in the range of ~1,000 K (1300 °F). Such a failure would yield natural depressurization, and avoidance of HP melt ejection altogether. The so-made transition to a LP scenario would make available the GDCS for safety injection, thus possibly arresting the meltdown process.

We also show that UDW liner failure due to thermal loads is physically unreasonable, while for the LDW liner such failures cannot be excluded. However the ESBWR liner and the air-gap behind it are compartmentalized, providing a significant degree of isolation from such local failures, and thus providing a major interference to the flow path to the outside of containment. This is reflected in the HP CPET (Section 21.6), and the Level-3 PRA.

Table 21.3.5-1

Nomenclature to Section 21.3 (DCH)

a_{s0}	Sound speed of steam
A_b	Area of vessel breach
$A_{connect}$	Area connecting LDW and UDW
C_p	Specific heat at constant pressure
C_v	Specific heat at constant volume
H	Height of vertical vents
L	Length of horizontal vents
m	Mass
$\dot{m}$	Mass flow rate
M	Molecular mass
P	Pressure
Q_{ox}	Heat generated by oxidation of 1kg melt
t	Time
T	Temperature
V	Volume
x_i	Position of water slug in horizontal vent i
z	Position of water slug in vertical vents
$Z_{i,h}$	Vertical elevation of horizontal vent row i

Greek letters

β	Virtual mass coefficient
η	Discharge coefficient
η_{nc}	Fraction of non-condensable gas
ρ	Density
τ_m , τ_e	Melt entrainment time during DCH
τ_s	Blowdown time
ν	Stoichiometric coefficient of oxidation reaction
ψ_{WW}	Effectiveness of gas-coolant heat transfer in SP

Table 21.3.5-1 Nomenclature to Section 21.3 (DCH) (cont'd)

Subscripts

conv	Convective transport between LDW and UDW
LDW	Lower drywell
m	Melt
Mix	Melt-blowdown steam mixture
RCS	Reactor coolant system
UDW	Upper drywell
WW	Wetwell
v	Vapor
0	Initial

21.3.6 References

21.3. -1 Allen, M.D., Pilch, M. M., Blanchat, T. K., Griffith, R. O., and Nichols, R. T. (1994), "Experiments to Investigate Direct Containment Heating Phenomena with Scaled Models of the Zion Nuclear Power Plant in the SURTSEY Test Facility," NUREG/CR-6044, SAND93-1049, Sandia National Laboratory, May 1994. Also in: The Integral Effects Test (IET-1) in the Surtsey Test Facility. 1991 Water Reactor Safety meeting; 28-30 Oct 1991; Washington, DC (SAND-91-2613C).

21.3. -2 Binder, J. L., McUmber, L. M., and Spencer, B. W. (1994), "Direct Containment Heating Integral Effects Tests at 1/40 Scale in Zion Nuclear Power Plant Geometry," NUREG/CR-6168, ANL-94/18, Argonne National Laboratory, September 1994.

21.3. -3 DYNA3D (2004). Code Manual. Lawrence Livermore National Laboratory.

21.3. -4 GE (1974). Mark III Confirmatory Test Program, Phase I - Large Scale Demonstration Tests, Test Series 5701 through 5703, NEDM-13377, October 1974.

21.3. -5 GE (1987; 1994) General Electric. Standard Safety Analysis Report (SSAR) for ABWR (1994 Final Submission version).

21.3. -6 GE-NE (2005a), ESBWR Certification Probabilistic Safety Assessment. NEDC-33201P. August 2005.

21.3. -7 GE-NE (2005b), ESBWR Design Control Document. 26A6642BZ Rev.00. August 2005.

21.3. -8 NRC (1994) U.S. Nuclear Regulatory Commission. “Final safety evaluation report related to the certification of the advanced boiling water reactor design”, NUREG-1503.

21.3. -9 OECD/NEA/CSNI (1996). High pressure melt ejection (HPME) and direct containment heating (DCH): state-of-the-art report, 1996.NEA/CSNI/R(96)25. OCDE/GD(96)194. Report prepared by Fauske and Associates Inc., Sandia National Laboratory in collaboration with NEA Group of Experts. 330p.

21.3. -10 Pilch, M.M., Yan, H. and Theofanous, T.G. (1996), “The Probability of Containment Failure by Direct Containment Heating in Zion,” Nuclear Engineering & Design, 164 (1996) 1–36.

21.3. -11 Pilch, M.M. and Allen, M. D. (1996) "Closure of the direct containment heating issue for Zion”, Nuclear Engineering & Design, 164, pp.37-60.

21.3. -12 Pilch, M.M. (1994), Continued Enlargement of the Initial failure Site in the Reactor Pressure Vessel. Appendix J in NUREG/CR-6075, SAND93-1535. Also, Nuclear Engineering and Design, 164 (1996).

21.3. -13 Pilch, M.M. (1996) "A Two-Cell Equilibrium Model for Predicting Direct Containment Heating”, Nuclear Engineering & Design, 164, pp.61-94.

21.3. -14 Pilch, M.M., Allen, M.D. and Williams, D.C. (1997) "Heat Transfer during Direct Containment Heating", V.29: Heat Transfer in Nuclear Reactor Safety. Elsevier, 1997.

21.3. -15 Rashid, Y.R. (1997), "Creep Considerations of the Lower Head", Nuclear Engineering & Design, 169, 101–108.

21.3. -16 Reddy, G.P. and Ayers, D.J. (1982), "High-Temperature Elastic-Plastic and Creep Properties for SA533 Grade B Class I and SA508 Materials", EPRI NP-2763, Electric Power Research Institute.

21.3. -17 Scobel, J.H., Theofanous, T.G., and Sorrell, S.W. (1998), "Application of the Risk Oriented Accident Analysis Methodology (ROAAM) to Severe Accident Management in the AP-600 Advanced Light Water Reactor," Reliability Engineering and Safety Systems, 62 (1998) 51-58.

21.3. -18 Smith, G.V. (1971), "Evaluation of the Elevated Temperature Tensile and Creep Rupture Properties of C-Mo, Mn-Mo, and Mn-Mo-Ni Steels", Metal Properties Council, American Society for Testing and Materials, ASTME Data Series Publication DS47.

21.3. -19 Theofanous, T.G. (1996), "On the Proper Formulation of Safety Goals and Assessment of Safety Margins for Rare and High-Consequence Hazards," Reliability Engineering & Systems Safety, 54 (1996) 243–257.

21.3. -20 Yan, H. and Theofanous, T.G., (1993), "The Prediction of Direct Containment Heating," ANS Proceedings 1993 National Heat Transfer Conference, Atlanta, GA, Aug. 8-11, 1993, 294-309.

21.3. -21 Yan, H. and Theofanous, T.G. (1996) "The Prediction of Direct Containment Heating," Nuclear Engineering & Design, 164 (1996) 95–116.

21.3. -22 Theofanous, T. G. Amarasooriya, W.H. Yan H. and Ratnam , U. (1991) "The Probability of Liner Failure in a Mark-I Containment," NUREG/CR-5423.

21.3. -23 Theofanous T.G. et al. (1993) "The Probability of Mark-I Containment Failure by Melt-Attack of the Liner," NUREG/CR-6025.

21.3.7 Quantification of DCH Loads (Addendum of July 31, 2006)

Subsequently to publication of this report, and as a result of internal audit checks, we found that due to miscommunication between this effort and other parts of systems design within the GE team, some of the basic inputs used in our evaluation of DCH loads had to be revised. The revised Table 21.3.4.3-4 is given as Table 21.3.4.3-4R. The purpose of this addendum is to supplement the previous quantification of DCH loads, using a completely verified set of reactor and containment design-related inputs. In addition, we take this opportunity to more explicitly relate the various sets of melt release conditions assumed in the calculations to respectively-consistent melt relocation, and RPV failure scenarios.

The design-related input revisions are as follows:

a. The volume of RCS (1,000 m^3, 35,300 ft^3) was taken as that of the SBWR (500 m^3, 17,700 ft^3), and the error was not caught in the original data audit because the ESBWR source (design) document was not available at the time.

b. Following a more detailed accounting of entities that occupy space in the wet-well, its free volume needed to be decreased from 5,400 m^3 (191,000 ft^3) to 5,000 m^3 (177,000 ft^3).

c. A typo in Table 21.3.4.3-4, showing the vent area as 16 m^2 (170 ft^2) is corrected to 13.6 m^2 (146 ft^2).

Scenario-related input revisions are summarized in the following. As determined in the"Mark I liner attack", ROAAM study (Theofanous et al, 1991, 1993), and confirmed by subsequent works, in BWRs, lower head failure is expected to occur in one of two possible, bifurcating scenarios. There is no way to assign relative probabilities to these, and thus in ROAAM we treat them both, independently, as "splinter scenarios".

a. Scenario I involves a sudden release of a significant fraction of the core (~10 to 30 %) into the lower plenum, this initial release being followed by gradual relocation of the remaining core mass at rates that are basically determined by the rate of melting. For DCH the significance of such a release (~4 to 12 m^3, ~140 to 420 ft^3) is that it would create the potential for immediate failure of one or more of the lower head penetrations (specifically by melting the welds on the instrument tube stubs), thus leading to an immediate high pressure melt ejection. Besides the melt quantity involved, this ejection would include the ~80 m^3 (2800 ft^3) of water found at that time in the lower plenum, and, subject to two-phase chocking, this ejection would last for 2 to 3 minutes—a time scale that is long enough to allow a great deal of thermal interactions at relatively low velocities, and thus a significant amount of quenching of the largely oxidic core debris, on the LDW floor, prior to it being subjected to the gaseous blow-down that would follow. Viewed in the light of the results presented originally (Table 21.3.4.3-6) it is rather obvious that Scenario I is not a significant DCH threat to containment integrity. Moreover, it should be quite clear that Scenario I would not lead to as significant temperature increases in the UDW, as found in the absence of water, perhaps not even in the LDW.

b. Scenario II involves gradual releases from the core region, ready quench inside the lower plenum, and negligible potential for early failure of lower head penetration

welds. Thus we expect that failure would require a dry-out and reheat cycle, and that it would occur much later, with essentially all the core debris found in the lower plenum. Failure would occur via melt attack by the superheated metallic components, mainly steel and Fe-Zr eutectics, while the oxidic contents are still mostly in solid state. Considering that total quantities present, ~50 metric tons (55 tons) of metallic Zirconium and ~80 metric tons (88 tons) of steel, and the large thermal gradients due to relocation, quenching, composition, and convection history effects, bounding estimates of metallic mass available for release upon failure may be taken as 30% of the above quantities; that is 15 metric tons (17 tons) of Zirconium and 25 metric tons (28 tons) of steel, in total 40 metric tons (44 tons) of metallic melt. Thus for a consistent, but bounding set of high pressure melt ejection conditions, the values in Table 21.3.4.3-5Ra were used for DCH load quantification.

c. In addition to the above, scenario-based definition, and for further perspectives on some of the cases shown previously in Table 21.3.4.3-5, calculations with a new set of release conditions, as found in Table 21.3.4.3-5Rb, and marked arbitrary-parametrics were carried out.

Since all basic behaviors and trends are as found and discussed in the first edition, results are summarized only in terms of peak pressures as shown in Table 21.3.4.3-6R. These results clearly verify and support our previous position on DCH loads, and thus our previous assessment of containment failure probability.

Table 21.3.4.3-4R
Geometry and Initial Conditions in Reactor Calculations
(Previous values in Table 21.3.4.3-4, when different, are shown in brackets)

Compartment	Parameter	Definition	Value
Primary System	V_{RCS}, m^3 (ft^3)	Volume of RCS	900 (32,000) [500(17,700)]
	P^0_{RCS}, MPa (psia)	Pressure of RCS at blowdown	8.5 (1230) [8.0 (1160)]
	T^0_{RCS}, K (°F)	Temperature of RCS at blowdown	800 (980)
	fH_2:fN_2:fH_2O	Gas molar composition (%)	0:0:100
Upper Drywell (UDW)	V_{UDW}, m^3(ft^3)	Volume of upper drywell	6016 (212,500)
	P^0_{UDW}, MPa (psia)	Initial pressure of UDW	0.25 (36)
	T^0_{UDW}, K (°F)	Initial temperature of UDW	420 (300) [300 (80)]
	fH_2:fN_2:fH_2O	Gas molar composition (%)	25:65:10 [0:0:100]
	$A_{connect}$, m^2 (ft^2)	Area connecting upper and lower compartment through convection	14 (150)
Lower Drywell (LDW)	V_{LDW}, m^3 (ft^3)	Volume of lower compartment	1,190 (42,000)
	P^0_{LDW}, MPa (psia)	Initial pressure of LDW	0.25 (36)
	T^0_{LDW}, K (°F)	Initial temperature of LDW	390 (242) [300 (80)]
	fH_2:fN_2:fH_2O	Gas molar composition (%)	10:80:10 [0:100:0]

Wetwell	A_{pool} , $m^2(ft^2)$	Total area connecting the upper compartment to the suppression pool	13.6 (146)
	D_{vent} , m (in)	Diameter of horizontal vent	0.7 (28)
		Number of rows of horizontal vents	3
		Distance vent rows	1.37 (53.9)
	H , m (in)	Height of water for clearing	5.45 (17.9)
	$V_{WW,}$ $m^3(ft^3)$	Wetwell (free) volume	5,000 (177,000) [5,400 (191,000)]
	P^0_{WW}, MPa	Initial pressure of WW	0.25 (36)
	T^0_{WW}, K (°F)	Gas temperature in wetwell	370 (206) [300 (80)]
	fH_2:fN_2:fH_2O	Gas molar composition (%)	50:35:15 (0:100:0)

Table 21.3.4.3-5Ra

Release Conditions and Variables used in Reactor Scenario-Based Bounding Calculations

Parameter	Parameter Definition	Bounding Case		
		A	B	C
m_m^0 metric tons (tons)	Initial mass of corium in the lower drywell (Scenario II, metallic melt)	40 (44)	50 (55)	50 (55)
D_S, m (in)	RPV hole size for steam blowdown	0.2 (8)	0.2 (8)	0.3 (12)
T_{RCS}^0 K(°F)	Initial temperature	2300 (3700)	2200 (3500)	2200 (3500)
τ_m (s)	Mixing time between melt and blowdown steam	10	15	10

Table 21.3.4.3-5Rb

Release Conditions and Variables used in Arbitrary-Parametric Calculations.

Parameter	Parameter Definition	Bounding Case				
		V	W	X	Y	Z
m_m^0, metric tons (tons)	Initial mass of corium in the lower drywell (oxidic/metallic melt)	100 (110)	100 (110)	100 (110)	300 (330)	300 (330)
T_{RCS}^0 (K) (°F)	Initial temperature	2400 (3900)	2400 (3900)	3000 (4900)	2400 (3900)	2400 (3900)
D_S, m(in)	RPV hole size for steam blowdown	0.2 (8)	0.3 (12)	0.3 (12)	0.3 (12)	0.5 (20)
τ_m (s)	Mixing time between melt and blowdown steam	20	10	10	12	8

* - In arbitrary-parametric calculations, the fraction of Zr is selected to reflect the material composition in full core, accounted for Zr oxidation prior to DCH (f_{Zr} =0.15)

Note: A set of common parameters used in all of these calculations includes:

Φ - Fraction of metal in entrained melt participating in steam-metal oxidation during blowdown; Φ = 0.5

α - Fraction of blowdown steam interacting with melt; α = 1.0

ψ_{WW} - - Effectiveness of gas-coolant heat transfer in the suppression pool; ψ_{WW} =0.9.

$f_{H_2O}^{condense}$ - Efficiency of steam condensation in the suppression pool; $f_{H_2O}^{condense}$ =1.

Table 21.3.4.3-6R

Summary of Results of Reactor Calculations

Parameter	Parameter Definition	Bounding Case			Arbitrary Case				
		A	B	C	V	W	X	Y	Z
P_1 bar (psia)	First (before vent clearing) pressure peak	3.2 (46)	3.2 (46)	4.0 (58)	3.3 (48)	4.2 (61)	4.5 (65)	4.2 (61)	6.5 (94)
P_2 ,bar (psia)	Second pressure peak	5.0 (73)	5.8 (84)	6.8 (99)	7.0 (102)	7.3 (106)	8.0 (116)	7.7 (112)	10.1 (146)
P_∞ ,bar (psia)	Long-term pressure	5.7 (83)	6.3 (91)	7.7 (112)	7.4 (107)	8.1 (117)	8.6 (125)	8.5 (123)	10.8 (157)
T_{STAB} ,K (°F)	Stabilized temperature	750 (890)	850 (1070)	800 (980)	1000 (1340)	900 (1160)	980 (1300)	1000(1340)	1050 (1430)